Durham E-Theses

The production and decay of sigma hyperons by kaons at rest

Abdullah, Muzahim Mohammed

The Production and Decay of Sigma

Hyperons by Kaons at Rest

A Thesis presented

by

MUZAHIM MOHAMMED ABDULLAH
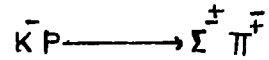
for the

Degree of Master of Science

at the

University of Durham

September 1977

TO MY PARENTS

ABSTRACT

A sample of 22354 $\bar{K}$-meson interactions at rest leading to the channels

$$\bar{K} P \longrightarrow \Sigma^{\pm} \pi^{\mp}$$

has been obtained from an exposure to the British National Hydrogen Bubble Chamber containing a track sensitive target. The data have been used to determine Γ, which is the ratio of the production of Σ^{-} hyperons to the production of Σ^{+} hyperons. The quantity B, which is the branching fraction of Σ^{+} hyperons into positive pions has been determined simultaneously.

The value of B ($=0.487 \pm 0.008$) is in close agreement with the known world value which gives confidence in the sample and in the method that have been used to determine B and Γ. The value of Γ ($=2.35 \pm 0.07$) resolve the existing discrepancy between the known measured values.

This thesis contains a description of the importance of Γ, an account of the experiment including a detailed consideration of how the ratios were determined.

CONTENTS

LIST OF FIGURES   Following page

LIST OF TABLES

CHAPTER ONE   THE RATIO, Γ

1.1   Introduction

There have been several attempts to study $\bar{K}P$ interactions (ref.1,2,6)

at low momenta within the momentum range (0-550)Mev/c.   Because this

momentum range limits the experimental technique almost entirely to the

bubble chamber method, the statistical weights of the experiments,

particularly the early ones, tend to be low.   The reactions which occur

chiefly are:

$$K\,P \longrightarrow \bar{K}^- P \qquad (1)$$
$$\longrightarrow \bar{K}^o n \qquad (2)$$
$$\longrightarrow \Sigma^- \pi^+ \qquad (3)$$
$$\longrightarrow \Sigma^+ \pi^- \qquad (4)$$
$$\longrightarrow \Sigma^o \pi^o \qquad (5)$$
$$\longrightarrow \Lambda \pi^o \qquad (6)$$
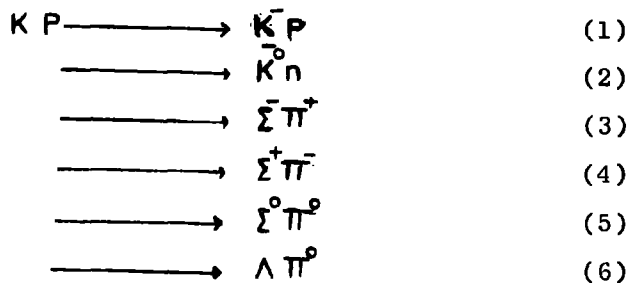
Although the $\bar{K}P$ reactions are dominated by three sets of two body final

states $\bar{K}N$, $\Sigma\pi$ and $\Lambda\pi$, multipion production (e.g.$\Sigma\pi\pi$, $\Lambda\pi\pi$) is

possible, but in the low momentum region it amounts to less than 1% of

the total cross section.   With charge independence the reactions above

involve the two isopin states $T = 0$ and 1, whereas reaction 5 occurs in

isopin $T=0$ and reaction 6 is isopin $T = 1$.

Models of the K-matrix type have been developed by Dalitz and Tuan   (3)

and others for the analysis of the low momentum data on the K-interaction

Unfortunately the experimental data are insufficient to allow a determination

of the K-matrix parameters.   Instead an s-wave, constant-scattering length

parameterisation has been used which involves 6 quantities only and which

can be determined from the cross-section of the six reactions above. In this

parameterisation of the $K N$ reaction given by Dalitz and Tuan, the $\bar{K}P$ elastic

and charge exchange cross-sections are expressed in terms of two complex

constant scattering lengths, $A_o = a_o + ib_o$ and $A_1 = a_1 + i\,b_1$ for the isopin

0 and 1 channels respectively.   Besides these four real parameters contained

in Ao and A_1, two more parameters are necessary to express the observed kaon cross sections. These parameters are chosen as a) the ratio (ϵ) of the $\Lambda \pi^o$ production rate to the total hyperon rate in the isopin 1 channel and, b) the phase angle between the isopin 0 and 1 amplitudes.

Then the kaon cross-sections are(reference 1)

$$\frac{d\sigma_{Kp}}{d\Lambda} = \left| \frac{\csc\theta/2}{2Bk^2}\exp\left[\frac{2i}{kB}\ln\sin\theta/2\right] + c^2/2\frac{A_o+A_1-2ik_oA_oA_1}{D} \right|^2 \tag{7}$$

where θ is the scattering angle

$$\sigma_{\bar{K}n} = \frac{\pi k_o C^2}{k^2}\left|\frac{A_1-A_o}{D}\right|^2 \tag{8}$$

$$\sigma_{\Sigma^+\pi^-} = \frac{1}{6}\sigma_o + \frac{1}{4}(1-\epsilon)\sigma_1 - \sqrt{\frac{1}{6}\sigma_o\sigma_1(1-\epsilon)}\cos\phi \tag{9}$$

$$\sigma_{\Sigma^-\pi^+} = \frac{1}{6}\sigma_o + \frac{1}{4}(1-\epsilon)\sigma_1 + \sqrt{\frac{1}{6}\sigma_o\sigma_1(1-\epsilon)}\cos\phi \tag{10}$$

$$\sigma_{\Sigma^o\pi^o} = \frac{1}{6}\sigma_o \tag{11}$$

$$\sigma_{\Lambda\pi^o} = \frac{1}{2}\sigma_1\epsilon \tag{12}$$

In the above,

$D = 1 - i(k_o+c^2k(1-i\lambda))\frac{1}{2}(A_o+A_1)-k_o(c^2k(1-i\lambda))A_oA_1$,

k_o = the wave number (centre-of-mass ystem) of the $\bar{K}n$ channel (taken as $i/k_o/$ below $\bar{K}n$ threshold), k = the centre-of-mass wave number of K^-p channel, c^2 = the coulomb penetration factor = $(2\pi/kB)(1-\exp(-2\pi/kB))^{-1}$, B is the Bohr absorption cross-section in the T= o, T = 1 channels.

In these expressions the ratio (ϵ) is given by

$$\epsilon = \frac{\sigma_\Lambda}{\sigma_1} = \frac{q_\Lambda|N_1|^2}{q_\Sigma|M_1|^2+q_\Lambda|N_1|^2} \tag{13}$$

and the phase angle is defined by

$$\phi = \text{Arg}\left[\frac{M_o(1-ik_oA_1)}{N_1(1-ik_oA_o)}\right] = \phi_{th} + \text{Arg}\left(\frac{1-ik_oA_1}{1-ik_oA_o}\right) \tag{14}$$

where $\Phi_{th} = \text{Arg} \left(\dfrac{Mo}{M_1}\right)$ is the phase difference at $\bar{K}N$ threshold and Mo, M_1 and

N_1 are the reaction amplitudes in T = 0 and 1 states for Σ (Mo,M_1) and Λ(N_1)

respectively.

Dalitz and Tuan found with the then existing data that two solutions

fitted the data above threshold. Subsequently with the data of Kim[1]

one solution was eliminated. For the acceptable solution Kim's parameters

are

$$a_o = -1.674 \pm 0.038 \text{ fm}, \qquad bo = 0.729 \pm 0.04 \text{fm}$$

$$a_1 = -0.070 \pm 0.058 \text{ fm}, \qquad b_1 = 0.688 \pm 0.33 \text{fm}$$

$$E = 0.318 \pm 0.021 \qquad \Phi_{th} = -53.8^{\circ}$$

The main result of the scattering length fits is the prediction from the

negative value of a_o of a $\bar{K}p$ bound state which is identified as the Λ (1405)

resonance. Its presence must be taken into account in the determination

of the $\Lambda\bar{K}N$ and $\Sigma\bar{K}N$ coupling constants g_Λ^2 and g_Σ^2 from forward $\bar{K}N$ dispersion

relations (reference 4).

To study the region below threshold (assuming that extrapolation of

the amplitudes from the physical region to unphysical region is possible)

the data for $\bar{K}$ absorption at rest can be considered (that is when,

a kaon in a mesic atom undergoes capture by virtual nucleons bound in the

nucleus).

The Γ -ratios, ($\Gamma = \Sigma^-$ production/ Σ^+ production) have been observed

for $\bar{K}$ capture in some heavy nuclei, (reference 4) and are displayed as

$1/\Gamma$ in Figure 1 . The ratio has been measured in deuterium ($\Gamma = 1.14 \pm 0.13$),

helium ($\Gamma = 0.29 \pm 0.03$), and in nuclear emulsion using heavy nuclei

($\Gamma = 0.84 \pm 0.09$) and light nuclei ($\Gamma = 0.58 \pm 0.06$). They are compared

with the value for hydrogen in Figure 1 . Also shown in the figure are the

expected values of Γ assuming various scattering length models. The values of

centre of mass energy below threshold are uncertain. They are estimated

from the average energy that would be needed to extract the proton (on
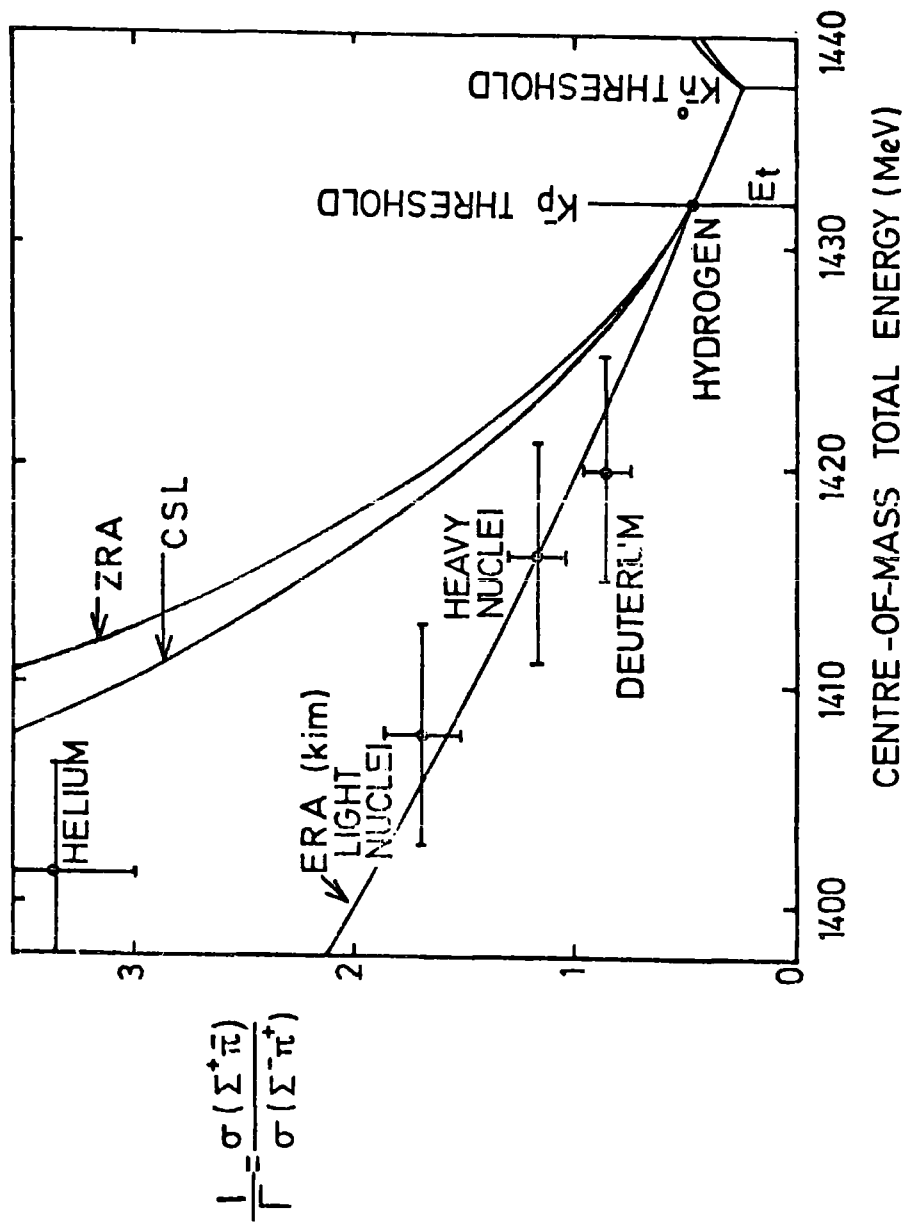
FIG. 1. A COMPARISON OF THE RATIO $\sigma(\Sigma^+\pi^-)/\sigma(\Sigma^-\pi^+)$ CALCULATED BY EXTRAPOLATING THE $\bar{K}p$ SOLUTIONS BELOW THRESHOLD WITH THE VALUES OBTAINED FROM THE K^- NUCLEAR CAPTURE DATA.THE CURVES ARE EXPECTED VALUES FOR $1/\Gamma$ FOR THE EFFECTIVE RANGE APPROXIMATION(ERA);ZERO RANGE APPROXIMATION(ZRA) AND CONSTANT SCATTERING LENGTHS(CSL).

which the capture occurs) from the nucleus.   Many factors have been

neglected such as secondary interactions in the same nucleus (e.g. $\Sigma P \longrightarrow \Lambda n$ OR

$\Sigma^o n$, $\Sigma^+ n \longrightarrow \Lambda P$ OR $\Sigma^o P$) multiple scattering, and the possibility

of real Y* production (reference 3).

The ratio is of prime importance in the establishment of the $\bar{K}N$ reaction

matrix since it determines the relative phase between the T=0 and T=1

amplitudes in the channel.   In fact if the behaviour of this ratio below

the $\bar{K}P$ threshold could be reliably set free from the effect introduced by

the presence of other various nuclear properties,   a study of ($\Sigma^{\pm} \pi^{\mp}$)

production in nuclei could provide results of great interest in the region

just below $K\bar{p}$ threshold ($\Lambda(1405)$) and would differentiate between solutions

of the K-matrix which only diverge appreciably below the $\bar{K}P$ threshold.

The value of Γ in hydrogen at threshold has been determined by Kim(1)

using a hydrogen bubble chamber.   The value was found to be (2.06$\pm$ 0.06).

It has also been determined by Tovee (5) using the hydrogen in nuclear

emulsion where the value is (2.34 $\pm$ 0.08).   (As a general observation it

is interesting to note that there are only two experimental studies with

relatively high statistics of the Kp interation at low momenta (P_K^- 300Mev/c)

(reference 6), but only one, that of Kim, involves a study of all final states.)

The two results above differ   by about three standard deviations.

Because of this experimental situation and because of the importance of Γ

to extrapolation into the non-physical region, a further determination of

this ratio should be made.   The method of analysis adopted by Kim in

determining the ratio Γ for $\bar{K}$-meson captures at rest on proton is not

clearly stated in his thesis. He only remarks that his sample comprised

(4994) Σ^- and (2429) Σ^+.   However if it is to be assumed that he used the

same range and angular selections of these data as he himself used when

determining the in-flight $\bar{K} P \longrightarrow \Sigma^{\pm} \pi^{\mp}$ cross-sections, (or those explicitly

stated by Chang (reference 7) when determining the $\Sigma^{\pm}$ hyperon lifetimes using

the same film), then the remark of Eisele (reference 8) is appropriate. This concerns the biases, arising from uncertainties in measurement errors when they are comparable with the length of the tracks measured and which are known to occur for lifetime measurements. Since the number of events excluded by a given short range cut ($\sim$1mm) on the track of a Σ hyperon is significant and moreover strongly dependent on the sign of its charge through the lifetime τ. ($\tau_{\Sigma^-} \sim 2\tau_{\Sigma^+}$) then uncertainty in the application of this length criterion will lead to larger effects with Σ^+ than with Σ^- hyperons. This is well illustrated by the results of a calculation given in table 1 . Those sigma hyperons produced in K^-p interations at rest are considered in a calculation where measurement errors on track length are taken into account via a gaussian distribution. The loss of events, when a minimum track length is required, is estimated and shown in table 1 . As can be seen the losses are substantial and larger for Σ^+ than for Σ^- The correction factor by which the observed ratio Γ should be multiplied is also shown. For errors in the range of 0.0 to 1.5 mm the correction factors themselves are uncertain from about 4% to 20%. Obviously without an exact knowledge of the size of the measuring accuracy it will not be possible to determine the ratio of Σ^-/Σ^+ to any great precision by using only those events in which the lengths of the sigma tracks are greater than some minimum value. From the results presented in table 1 it is evident that probably an unattainably precise knowledge of the measurement error is essential to make a sensible determination of Γ accurate to within a few persent by this method (lifetime method). In addition the measurement error in the $\Sigma^\pm$ production and decay points causes a considerable spreading out of the observed time distribution. This is illustrated in Figure 2 where the apparent life time of $\Sigma^\mp$ is shown as function of measuring error in mms. In the range of typical measuring errors (0.5-1mm) the apparent lifteime of the Σ^+ is increased by 4% and that of the Σ^- by 3%.

TABLE. 1.

CUT OFF (mm)	ZERO ERROR			ERROR 0.5 mm			ERROR 1.0 mm		
	$\bar{\Sigma}$ %	Σ^+ %	$\bar{\Sigma}/\Sigma^+$ % CORRECTION	$\bar{\Sigma}$ %	Σ^+ %	$\bar{\Sigma}/\Sigma^+$ % CORRECTION	$\bar{\Sigma}$ %	Σ^+ %	$\bar{\Sigma}/\Sigma^+$ % CORRECTION
0.5	7.2	12.0	0.948	5.5	9.0	0.958	4.3	7.0	0.971
1.0	13.8	24.0	0.882	11.2	19.5	0.907	9.5	15.0	0.939
1.5	20.3	35.5	0.809	17.4	27.5	0.878	14.3	23.0	0.898
2.0	26.4	47.5	0.713	22.8	39.0	0.790	19.9	31.5	0.855

PERCENTAGE LOSSES AND CORRECTION FACTORS OF $\Sigma^{\pm}$ HYPERONS WHEN A MINIMUM OBSERVABLE LENGTH IS REQUIRED,(CUT OFF LENGTH),IN THE PRESCENCE OF MEASURING ERRORS OF 0, 0.5 AND 1.0mm.
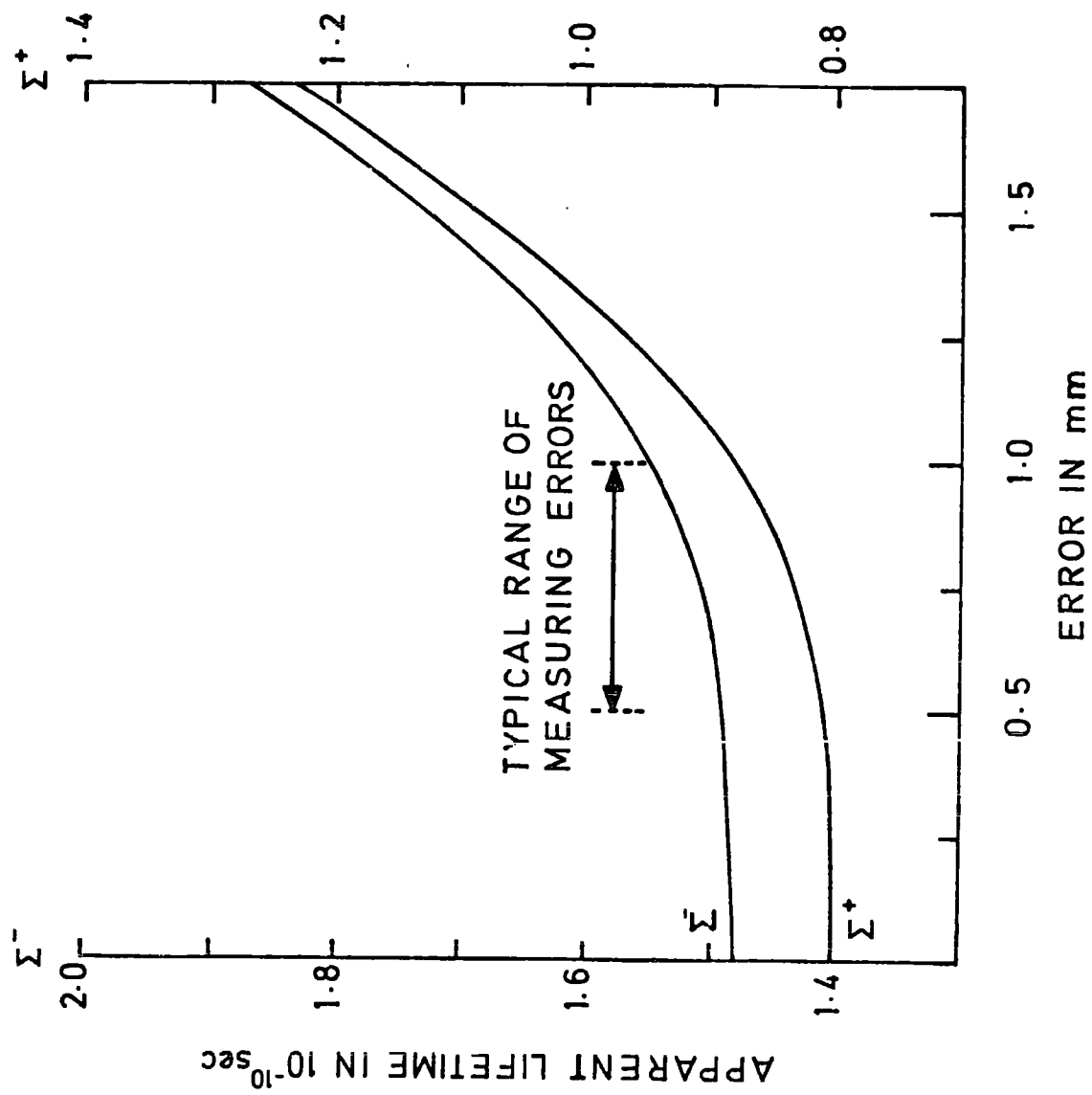
FIG. 2 THE APPARENT LIEFTIME AS A FUNCTION OF MEASURING ERROR

1.2 Methods of Determining Γ

Two methods of determining Γ will be employed. In the first of these the objection, discussed above to the use of events where the Σ – hyperons are larger than some minimum length, is overcome by using all Σ – hyperon events above and below the minimum length. In the second method, essentially a minimum length is determined which corresponds to an effective zero measuring error.

a) Method one

This method of analysis avoids any range and angular selections and consequently biases associated with them. The major difficulty is that at low energy, Σ_S have short lengths before decay and so in some $\Sigma^{\pm} \pi^{\mp}$ events the $\Sigma^{\pm}$ is not visible and only the production and decay pions are seen ($\pi^{+} \pi^{-}$ events). The philosophy of this method is to avoid attempting to separate the $\pi^{+} \pi^{-}$ events, by scanning and measuring, into Σ^{-} and Σ^{+} categories. Instead the number of Σ^{+} decaying into pions is determined from the number decaying into protons through the known branching ratio

$$B = \frac{\Sigma^{+} \longrightarrow \pi^{+} n}{\Sigma^{+} \longrightarrow P \pi^{0} + \Sigma^{+} \longrightarrow n \pi^{+}}, \quad (B = 0.4835 \pm 0.007) \text{ (reference 9).}$$

It is necessary to define categories of events as follows:

$N_{\Sigma^{-}_{\pi}}$ – expected number of $\Sigma^{-} \longrightarrow \pi^{-} n$ decay.

$N_{\Sigma^{-}_{\pi}}(obs)$ – observed number of such decays where the Σ^{-} is seen.

$N_{\Sigma^{-}_{\sigma}}(obs)$ – observed number of Σ^{-} absorption.

$N_{\pi^{+}\pi^{-}}(obs)$ – observed unresolved $\pi^{\pm} \Sigma^{\mp} (\longrightarrow \pi^{\mp} + n)$ events where the $\Sigma^{\pm}$ cannot be seen.

$N_{\Sigma^{+}_{\pi}}$ – expected number $\Sigma^{+} \longrightarrow \pi^{+} n$ decays.

$N_{\Sigma^{+}_{\pi}}(obs)$ – observed number of such decays where the Σ^{+} is seen.

$N_{\Sigma^{+}_{P}}(obs)$ – observed number of $\Sigma^{+} \longrightarrow P \pi^{0}$ decays.

$N_{\pi P}$ – observed number of Σ^{+} decay to $P \pi^{0}$ where the Σ^{+} is not seen.

From these categories the total numbers N^+, N^- of Σ^+ & Σ^- events can be calculated from which $\Gamma = N^-/N^+$

Firstly,

$$N^+ = N_{\Sigma^+ \to p}(obs) + N_{\pi^- p} + N_{\Sigma^+ \to \pi}(obs) + f_+ (\pi^+ \pi^-) \quad \dots\dots(15)$$

where f_+ is an unknown fraction of the $\pi^+ \pi^-$ events. However, from the ratio, B, the last terms of the right hand side of equation (15) can be replaced and

$$N^+ = \frac{N_{\Sigma^+_p}(obs) + N_{\pi p}}{1 - B} \quad (16)$$

Secondly,

$$N^- = N_{\Sigma^-_\sigma}(obs) + N_{\Sigma^-_\pi} \quad (17)$$

$$= N_{\Sigma^-_\sigma}(obs) + N_{\Sigma^-_\pi}(obs) + f_-(\pi^+ \pi^-) \quad (18)$$

where f_- is an unknown fraction. It can be replaced and

$$N^- = N_{\Sigma^-_\sigma}(obs) + N_{\Sigma^-_\pi}(obs) + N_{\pi^+ \pi^-}(obs) - f_+ (\pi^+ \pi^-) \quad (19)$$

$$= N_{\Sigma^-_\sigma}(obs) + N_{\Sigma^-_\pi}(obs) + N_{\pi^+ \pi^-}(obs) - (N_{\Sigma^+_\pi} - N_{\Sigma^+_\pi}(obs)) \quad (20)$$

$$= N_{\Sigma^-_\sigma}(obs) + N_{\Sigma^-_\pi}(obs) + N_{\Sigma^+_\pi}(obs) + N_{\pi^+ \pi^-}(obs) - N_{\Sigma^+_\pi} \quad (21)$$

replacing $N_{\Sigma^+_\pi}$ as before

$$N^- = N_{\Sigma^-_\sigma}(obs) + N_{\Sigma^-_\pi}(obs) + N_{\Sigma^+_\pi}(obs) + N_{\pi^+ \pi^-}(obs) -$$
$$\frac{B}{1-B}\left[N_{\Sigma^+}(obs) + N_{\pi^- p} \right] \quad (22)$$

By this approach it is clear that accurate separation of $\Sigma \to \pi$ decays into Σ^- and Σ^+ is not necessary as long as the total number is counted. All that is required is an accurate estimation of the total number of $\Sigma^+ \longrightarrow p$ decays in the two cases where a) the Σ^+ is clearly visible and b) where the Σ^+ is not clearly visible but is readily identified by the proton involved in the decay. At the energies involved in this experiment there is no possibility whatsoever (except in the case of very steep tracks) where the π^+ and proton from Σ^+ decay can be confused. Hence the

accuracy of the determination of Γ is based on determining a clearly

recognisable decay. Except in a small number of cases no measurements

need to be involved since all judgements can be made at the scanning table.

Obviously the emphasis is on very high scanning efficiency and interpretation

of events. Consequently this kind of scanning has to be done by experienced

workers. In this experiment it was carried out by trained physicists.

b) Method two

In the previous method no attempt was made to divide the $\pi^+\pi^-$ events

into those originating from Σ^+ & Σ^- respectively. If it assumed that the

limit of resoltuion for detecting the decay of a Σ^-_π is exactly the same as

that for Σ^+_π then it is possible to divide the total number of $\pi^+\pi^-$

events into their charged Σ origins provided the limit of resolution can

be determined. Suppose that the effective length that a hyperon must

have before its charge can be recognised (by its decay secondary) is r,

than the Γ ratio can be calculated as follows:

The number of Σ^- seen to decay or be absorbed is

$$(N_{\Sigma^-_\pi}(obs) + N_{\Sigma^-_\sigma}) = N_{\Sigma^-}(\exp\frac{-t_-(r)}{\tau_-})$$ (23)

and the corresponding number of Σ^+_π decays is

$$N_{\Sigma^+_\pi}(obs) = N_{\Sigma^+_\pi}(\exp\frac{-t_+(r)}{\tau_+})$$ (24)

where τ_-, τ_+ are the respective mean lives, t_- and t_+ are the respective times

to travel distance r ($t_- \sim 1.055\ t_+$). Assuming, as in method (1), that

the number of Σ^+ decays to proton is well determined and is given by

$N_{\Sigma^+_p}$ then

$$\Gamma = \frac{N_{\Sigma^-_\pi}}{N_{\Sigma^+_\pi} + N_{\Sigma^+_p}} = \frac{(N_{\Sigma^-_\pi}(obs) + N_{\Sigma^-_\sigma})e^{t_-(r)/\tau_-}}{N_{\Sigma^+_\pi}(obs)e^{t_+(r)/\tau_+} + N_{\Sigma^+_p}}$$ (25)

The effective length, r, is determined from the number of observed

events as follows.

$$N_{\pi^+\pi^-} = N_{\Sigma^-} (1 - \exp \frac{-t_-(r)}{\tau_-}) + N_{\Sigma^+_{\pi}} (1 - \exp \frac{-t_+(r)}{\tau_+}) \tag{26}$$

$$= (N_{\Sigma^-_{\pi}}(obs) + N_{\Sigma^-_{\sigma}})(\exp \frac{t_-(r)}{\tau_-} - 1) + N_{\Sigma^+_{\pi}}(obs)(\exp \frac{t_+(r)}{\tau_+} - 1) \tag{27}$$

In this expression only r is unknown and hence it can be determined from

the observed numbers of $\pi^+\pi^-$, Σ^-_{π} , Σ^-_{σ} and Σ^+_{π} events. Obviously,

by substituting r back into the two right hand terms of equation (26), the

numbers of $\pi^+\pi^-$, events are divided into those originating from Σ^- and

Σ^+ respectively.

With this value of r substitution into equation (25) will yield

the new estimate of Γ.

Furthermore, with the $\pi^+\pi^-$ events effectively separated it is possible to

determine the branching ratio of the Σ^+ into pions and protons where

$$B = \frac{N_{\Sigma^+_{\pi}}(obs) + f_+ N_{\pi^+\pi^-}}{N_{\Sigma^+_{\pi}}(obs) + f_+ N_{\pi^+\pi^-} + N_{\Sigma^+_p}} = \frac{N_{\Sigma^+_{\pi}}(obs) e^{t_+(r)/\tau_+}}{N_{\Sigma^+_{\pi}}(obs) e^{t_+(r)/\tau_+} + N_{\Sigma^+_p}} \tag{28}$$

Hence the attraction of this second method is that it yields a new estimate of

Γ and also a new estimate of B.

1.3 Summary

An account has been given of the relevance of the determination of

the ratio.

$$\Gamma = \Sigma^-/\Sigma^+$$

to the low momentum interactions of kaons. The experimental discrepancy has

been presented and two methods for further determination have been discussed

in outline.

In the further parts of this thesis an account is given of the experimental

application of those two methods. Firstly however the track sensitive

target chamber that has been used is described together with an account of

the experimental runs and exposures.   This is followed by a description
of the scanning and measuring that was made and terminates with a
discussion of the quality of the data.   Finally, there is a discussion
of the precision of the two methods of analysis leading to the final
determination of Γ and the branching ratio B.   In conclusion there
is a short discussion and comparison of Γ with other experimental results
and an indication is given of further work in this field.

CHAPTER TWO ··· THE CHAMBER AND EXPOSURE

2.1 Introduction

The work described in this thesis is part of a general experiment on the interaction of low momentum kaons. In Chapter 1 the main reactions were described (equation 1 to 6). In particular reactions 5 and 6 involved the production of π^0 mesons and were given by

$$K^- P \longrightarrow \Sigma^0 \pi^0 \qquad (5)$$

$$K^- P \longrightarrow \Lambda^0 \pi^0 \qquad (6)$$

In reaction (5) the Σ^0 decays very rapidly ($\tau \sim 10^{-16}$ sec) into $\Lambda \gamma$. Consequently as seen in the normal hydrogen filled chamber these two reactions appear to be identical. What is seen in each case is a terminating kaon track with close by, a Λ -hyperon pointing to the track ending. Moreover, in measurement these reactions are very similar and there is a high degree of ambiguity between the interpretation of events consisting only of a kaon track with a pointing Λ .

To avoid this ambiguity (and hence being able to analyse pure T=0 and pure T=1 reactions) an attempt was made in this overall experiment to detect the γ rays associated with these reactions. If γ -detection is very efficient then the clear signatures of reaction 5 (3γ-rays) and reaction 6 (2γ-rays) lead to the resolution of the ambiguity.

In the conventional hydrogen filled chamber the radiation length X, is about 10m, which leads to γ materialisation in a few percentage of cases only ($<5\%$). In a heavy liquid filled chamber the radiation length, with a neon filling, for example, becomes about 25cm which leads to an increase in materialisation probability by a factor of about 40. Unfortunately the reduced radiation length also implies large coulomb scattering and

consequently measuring precision is lost.

In the present experiment an attempt was made to combine the advantage of light and heavy liquids by building a composite system of a hydrogen filled chamber inside a neon filled chamber (reference 10). The hydrogen is to be used for measurment of primary interaction vertices and secondary decay vertices and the neon is to be used to increase the probability of γ - materialisation.

Although this feature (γ - materialisation) is of no importance in the physics involved in determining the ratio $(\frac{\Sigma^-\text{production}}{\Sigma^+\text{production}})$ it does have experimental consequences by the limitations on track length which are set by the small volume of hydrogen. In the following sections the composite chamber will be described and special attention will be drawn to the advantages and disadvantages that it imposes on the experiment as a whole.

2.2. Description of the British National Hydrogen bubble chamber with Track Sensitive Target

The chamber figure 3 vessel is bounded by two-parallel windows of which the clear aperture is rectangular with semi-circular ends and having dimension 150cm by 50cm. The windows are 15.5cm thick and they are spaced 45 cm apart between the inner faces. Thus the effective volume of the chamber is about 300 litres (reference 11). The chamber is photographed in dark field by an array of three cameras with parallel axes, perpendicular to the camera side main window. The cameras are placed 1.4m away from the chamber.

A reference system in the chamber is provided by set of crosses ruled on the inner surface of the main windows and on the outer surface of the camera side window.

Brief description of operation.

The chamber is run in a magnetic field of 12.3k gauss. Under normal conditions the conventional chamber is filled with hydrogen, made liquid by temperature (27 K) and pressure (8 Atmospheres). On

Beam Entrance

C = Camera
F = Flash
M = Magnet
S = Shield of Hydrogen
V = Vacuum
W = Window

M

M

S

C

H₂

W W

C

S

S

F

F

F

M

M

V

| Im. | O | Im. |

SCALE
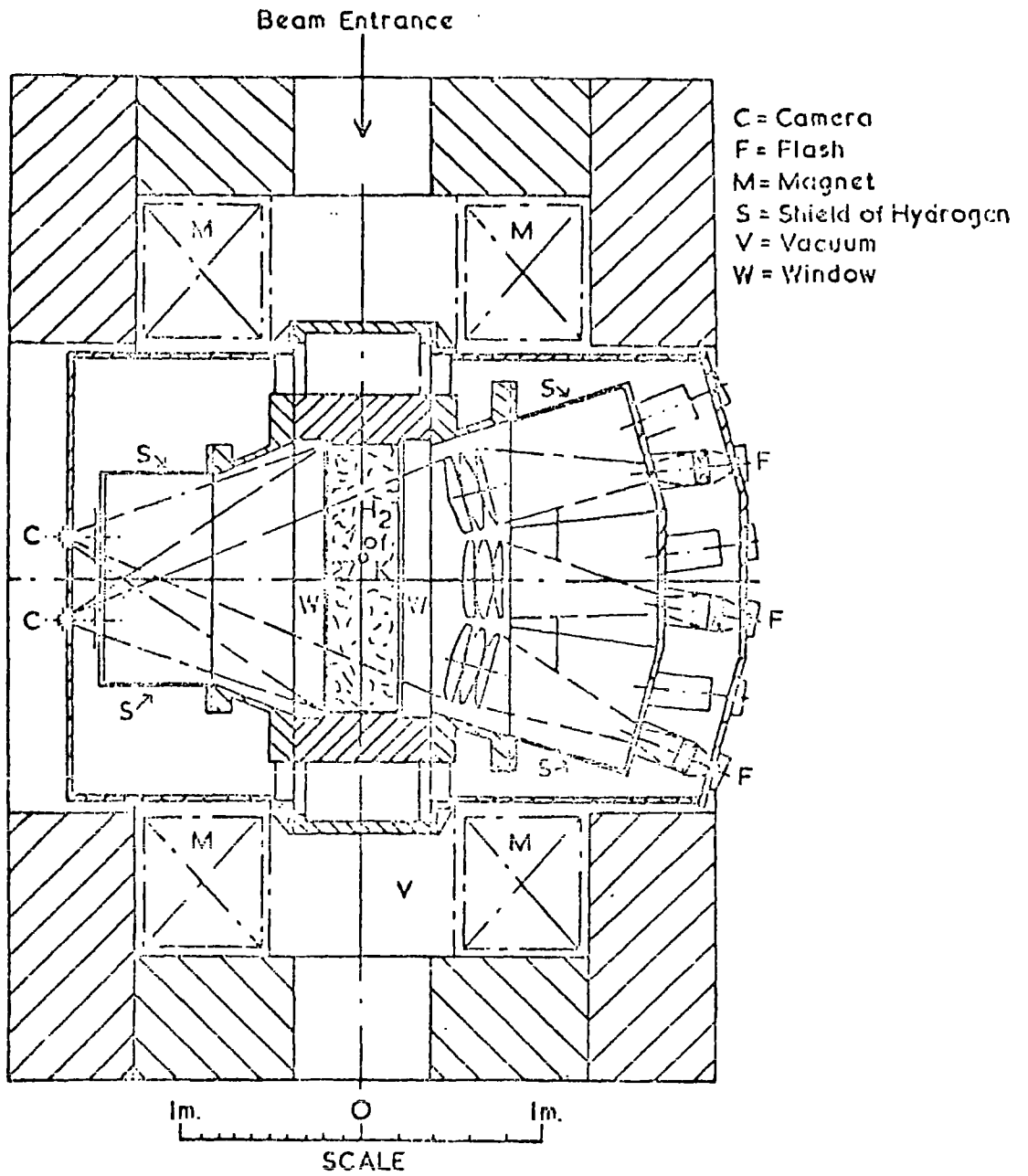
FIG. 3.   PLAN VIEW OF B.N.H.B.C. SHOWING
OPTICAL SYSTEM AND MAGNET

release of the pressure to about 4 Atmospheres the liquid hydrogen is now
at a temperature above its boiling point.   It can remain superheated for
a few m secs before spontaneous boiling will occur.   During this few milli
secs the beam of particles have to pass through the chamber, cause bubbles
to form at centres of ionisation, be photographed and the pressure restored
to make the liquid stable again.

However the chamber is used, in the composite system, under slightly
different conditions.   The chamber has been modified to enable it to be
used to with a target of liquid hydrogen surrounded by a neon-hydrogen mixture
 figure 4 .   The two liquids which can be made superheated and hence made
sensitive at a temperature of 29 K are separated by plexiglass windows which
are the walls of the target.   When the pressure of the outer part of the
chamber is reduced the flexing of the plexiglass walls tramsits the
necessary volume/pressure change to the hydrogen which also becomes sensitive.
The plexiglass windows on either side of the central plane of the chamber define
the depth of the T.S.T. as 7.85cm. The windows are 1.0cm thick.   Fiducial
marks are engraved on the outer surface of the T.S.T. walls.   Two track
sensitive targets have been successfully operated in the 1.5m cryogenic
bubble chamber at the R.H.E.L.   The first target was metal framed, whereas
the second was made completely out of plexiglass.

a)   Metal framed target:

The target (reference 12) consists of a strong stainless steel frame
which is rigidly mounted in the chamber body.
The plexiglass windows are sealed to the frame with a gasket of indium wires,
by inflating flexible steel tubes figure 5 .   The interal dimensions are
135. x 33.5 x 7.8 cm^3 and the external are 147 x 44.7 x 9.8cm^3 .
This target reduces the gamma detection efficiency since the metal frame
limits the useful visible region of the chamber.

walls of target

beam tracks enter
hydrogen only

target contains hydrogen

chamber contains
hydrogen mixture

tracks pass through
perspex into chamber

Gamma rays convert
to e⁺ e⁻ pairs in
neon hydrogen

Co-ordinate system, origin
at centre of chamber.
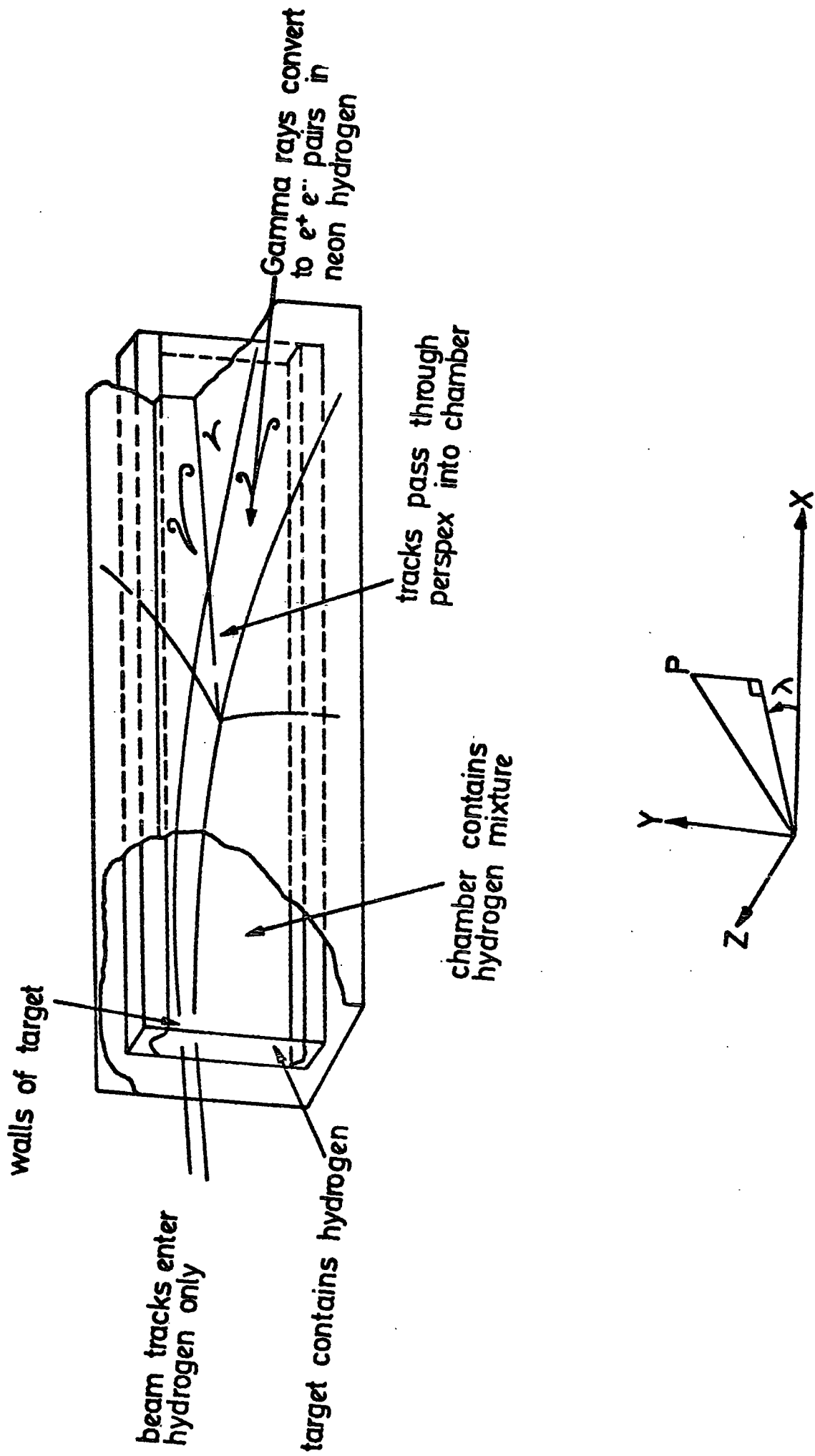
FIG. 4 SCHEMATIC DIAGRAM OF THE TRACK SENSITIVE TARGET INSIDE
THE BUBBLE CHAMBER.

Fig. 5 : The Composite target section. The beam enters directly into the hydrogen. The magnetic field produces a curvature in the plane of the target.
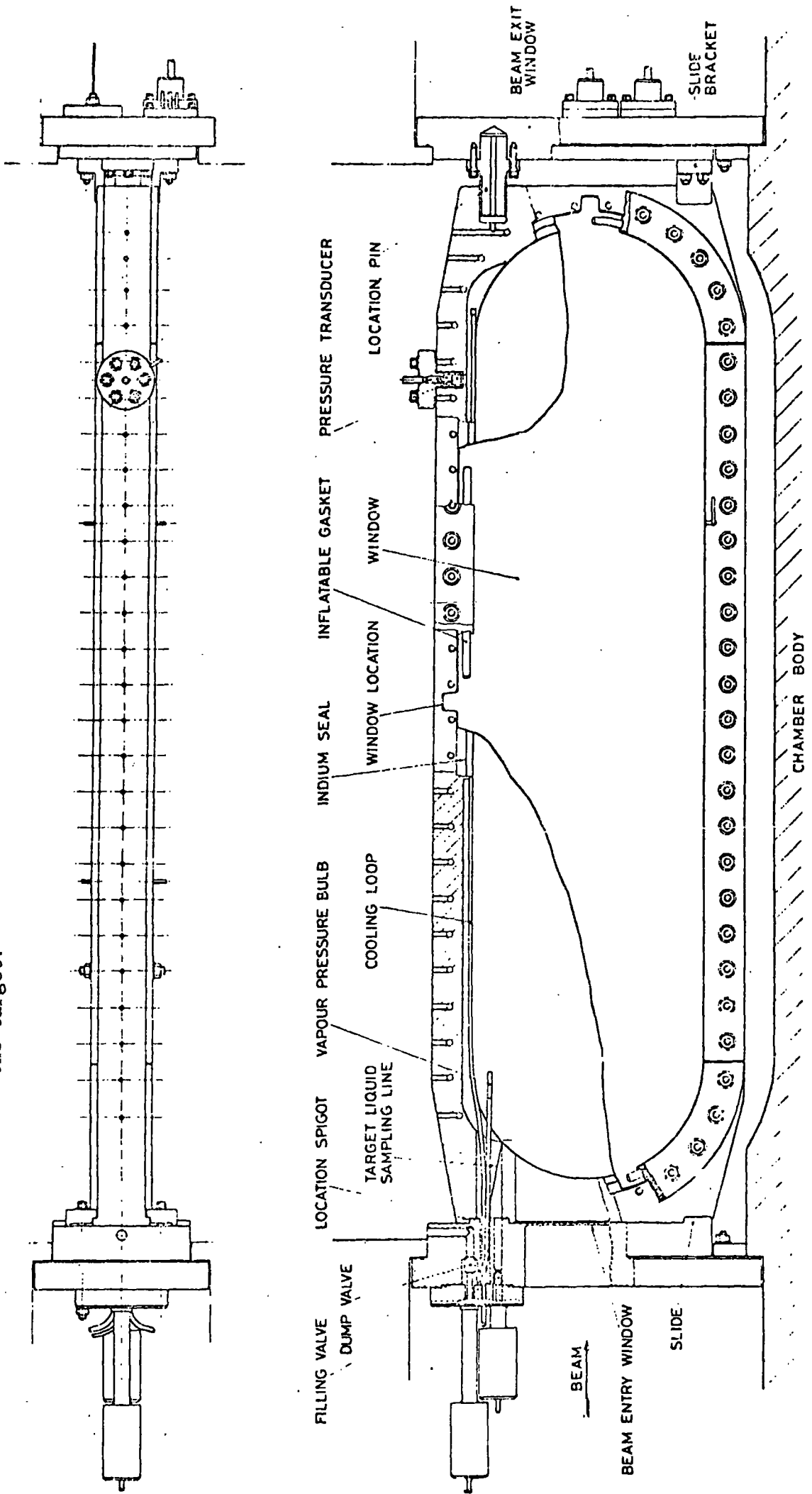
TRACK SENSITIVE TARGET FOR 1·5 METRE CHAMBER

FIG. 5

b) Plexiglass target (plastic framed target):

Since the composite target limited gamma detection, because of

obscuration by the metal frame, it was decided to build an all plexiglass

T.S.T. The essential simplicity of all plexiglass system is clear. The

plexiglass is transparent to both charged particles, gamma rays and visible

light and so the gamma efficiency is significantly increased. Whereas the

metal framed target was mounted parallel to the windows of the outer chamber,

the plexiglass T.S.T. was mounted at an angle to maximise the potential

path length of primary kaons in the T.S.T.

c) Neon-Hydrogen mixture

Experimentally it is found that neon cannot be made to work as a bubble

chamber liquid at a temperature close to the normal operation temperature

of hydrogen as a bubble chamber liquid unless the neon is diluted with

hydrogen. The richest mixture of neon-hydrogen that has been used is

about 80% by number density. In the present experiment the number density

varies from, initially about 70% to finally about 80%. In this range

of mixture the radiation length in Ne/H2 is about 45cm long compared to

the radiation length in hydrogen of 10m. This radiation length is smaller

by a factor of about 20. This implies that the conversion probability for

γ rays is increased by a factor of 20. Although this factor of 20

appears to be a very large increase it should be noted that this gives a

conversion probability of about 30% for a single γ ray in the composite

system described. Unfortunately, in this experiment (as distinct from

the first experiment with T.S.T. chamber with 4Gev pions), the γ

energies are quite low and in many cases the large energy loss and coulomb

scattering of the electron in the γ conversion make it impossible to

measure the γ energy. This reduces the effective conversion probability

to about 15%. Consequently the improvement by factor of 20 is reduced to

a factor of 10.

d)   T.S.T. Advantages and Disadvantages:

Several advantages are to be gained from using the T.S.T.   The main

advantage is the gain of γ conversions but at the same time, precision of

working in hydrogen is maintained, that is the target in unambigously a

proton and measuring precision is high.   Gamma rays from π^o, Σ^o...etc.decay

emerge through the perspex walls of the T.S.T. into the neon hydrogen

mixture where they may be converted into electron-positron pairs and

point to the production vertex.   In practice there is no difficulty in

associating gammas with the correct origin, although the electron and

positron tracks have the characteristic heavy liquid features of large

multiple scattering and bremsstrahlung.   The efficiency for multi-

gamma detection depends critically on the ratio of the conversion length

(9/7x radiation length) for gamma to the dimension of the bubble chamber

(reference 12).

The different track qualities in the two media are clear.   The bubble

size in the hydrogen turns out to be smaller ($\sim 200\mu$) than in a conventional

chamber and this leads to increased measuring precision and improved

resolution in the neighbourhood of vertices ($\sim 0.5mm$).   This is very

important in the determination of the Σ^-/Σ^+ ratio at rest, where the small

bubble size enables Σ^- & Σ^+ to be recognised   down to smaller lengths than

is usual in a hydrogen chamber.   There is a further gain in precision for

low momentum tracks which stop in neon.   For these, range rather than

curvature is measured leading to a considerable increase in precision.

A general visual advantage is gained at scanning time and that is that

the steepness of tracks can be judged quite accurately by the length of

the blank separation in plexiglass of the track hydrogen and its continuation

in neon.

The main disadvantage of the T.S.T. system is the small depth of the chamber (7.8cm). The low momentum kaon beams have been produced by passing higher momentum beams through a degrader of about 30 cm Aluminium. The emergent kaons are dispersed in both the horizontal and vertical directions and consequently the potential path length is quite low at 49cm. instead of 150 cm. At low momenta the secondary particles tend towards isotropy and the shallow depth immediately restricts the potential lengths.

In this particular experiment where 0 Λ (that is a zero pronged primary vertex with an associated Λ) events form an important topological group for the inflight interaction, about one half of the 0 prong events that are scanned are in fact primary interactions in the perspex.

The chamber depth is important in the determination of the Γ ratio at rest. In a conventional chamber where there is little depth restriction Σ^+ decay and Σ^- absorption are seen in their entirety (i.e. both primary and secondary vertices are seen). Here 1% of the secondary vertices occur in the T.S.T. walls because of narrowness of the chamber. To restrict events only to the central part of the chamber so that all events are complete would reduce the effective chamber depth by 25% which implies that 25% of the scanning in effect is made useless. Consequently, these incomplete events have to be used.

Normally at low momenta, Λ hyperons decay within a few cm of the vertex. Again with a shallow T.S.T. about 30% decay in the neon where curvature measurements are poor (because of coulomb scattering).

2.3 The exposure

The exposure took place in 1973 using a negative kaon beam transported at 600 meV/c directed into the hydrogen bubble chamber and degraded to lower momenta by an aluminium block mounted inside the sensitive target.

At the end of the exposure about 906000 frames with (5-20) $\bar{K}$ per frame had been obtained. An ideogram figure 6 of the approximate beam momentum is shown. The total kaon path length is about 1000 km.

The number of frames at each beam momentum is shown in table 2 . The films that have been used for results described in this thesis all come from the 229000 frames exposed to kaons largely at rest.

These films have been distributed among the following collaborating laboratories, Birmingham, Brussels, Durham, University College London and Warsaw University.
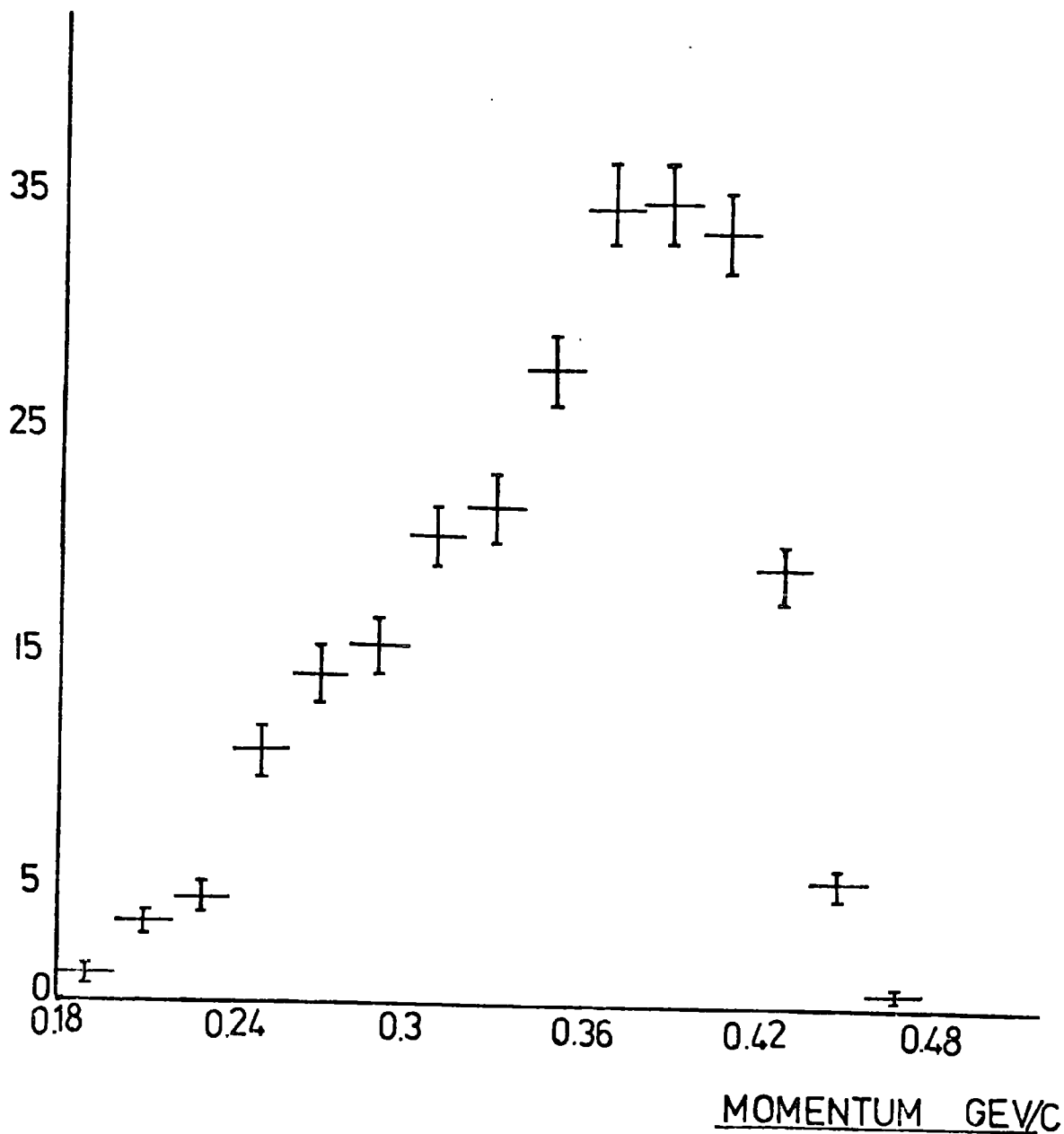
FIG. 6 IDEOGRAM OF APPROXIMATE BEAM MOMENTUM

Table 2

K19 Data taking summary

The experiment was divided into Blocks of film with differing external beam momentum, degrader thickness and target type.

Block No.	Roll Nos.	Thousands of frames	Approx. K⁻ per frame	Approx. entry momen. MeV/c	Approx. exit momen. MeV/c	Degrader thickness cms. AL	Target frame
1	1-105	229	5	260	0	30	metal
2	106-126	54	8·4	315	235	30	··
3	127-147	45	10·1	370	320	30	··
4	148-168	54	12·3	405	370	30	··
5	169-188	51	8·8	445	410	30	··
6	190-210	52	8·7	320	240	27	perspex
7	211-220	26	7·9	300	190	27	··
8	221-240	51	11·6	370	320	27	··
9	241-250	26	12·2	405	360	27	··
10	251-260	25	10·0	420	380	18	··
11	261-277	44	13·4	450	410	18	··
12	278-286	22	14·2	475	435	18	··
13	287-292	16	17·3	495	455	18	··
14	293-304	28	12·6	505	465	9	··
15	305-314	25	16·6	530	490	9	··
16	315-335	49	20·0	550	510	9	··
17	336-355	49	12·6	560	525	0	··
18	356-365	25	15 7	500	545	0	··
19	366-379	35	15 2	510	475	18	··

Total frames   906000 (229000 for stopping K̄)

CHAPTER THREE   SCANNING, MEASURING AND INITIAL DATA

It was emphasised in chapter 1 that the accurate determination

of Γ (i.e. Σ^- production/ Σ^+ production at rest) will depend on very

efficient scanning and accurate interpretation of events at the scanning

table.   Only $\sim$ 13% of the events need to be measured.

Since the GEOMETRY and KINEMATICS programmes (see Appendix 1,2) have

had to be modified to include the composite chamber and γ rays, and further

modifications have had to be made to handle very low momentum primaries it

has been necessary to measure considerably more events than envisaged to

test out thoroughly the changes that have been made.   Despite this the

precision of the experiment is still determined at the scanning stage.

3.1   Scanning Procedure

Each charged kaon entering the fiducial volume of the T.S.T. was

followed until it either interacted, left the hydrogen volume or left the

fiducial volume.   The fiducial volume is shown in Figure 7, it is very

restricted and ensures that all events recorded will have tracks long

enough for accurate measurement.   All events of interest were scanned in

at least two views.   A detailed record was made of the event and great

emphasis is placed on accuracy in the scan data since it is largely from

these that the Γ ratio is determined.

The classification into events "at rest" or "in flight" has also

been made.   Each roll of film has been scanned twice by physicists.   Any

discrepancies between the two scans were resolved in a final check scan.

a)   Classification of events

The events found were classified into two broad groups, 0 - prong

events and 2-prong events.   The 0 - prong events were only recorded if

they were accompanied by a K^0 decay in hydrogen (for later determination

of the charge exchange cross-section in flight), all 2-prong events were

recorded and were sub-divided into the following classes:-
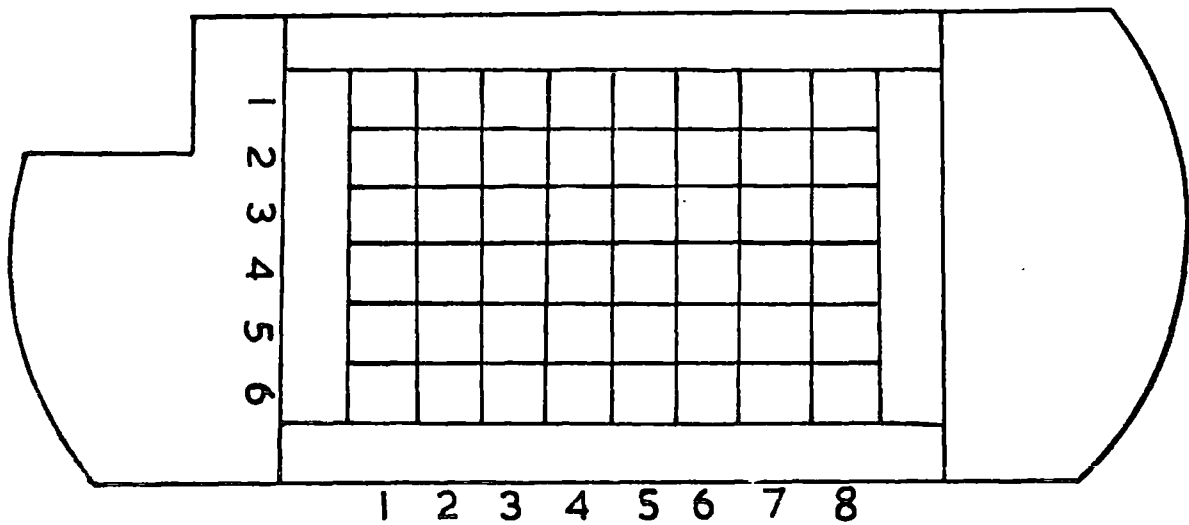
FIG. 7 SCANNING FIDUCIAL VOLUME

1) $K^-P \longrightarrow \Sigma^+\pi^-$ where the Σ^+ is seen as a visible track

and   is also seen to decay,

     a)   to a pion $- \Sigma^+_\pi$

or

     b)   to a proton $- \Sigma^+_p$

2) $K^-P \longrightarrow \Sigma^-\pi^+$ where the Σ^- is visible and is seen to,

     a)   decay to pion $- \Sigma^-_\pi$

or

     b)   to be absorbed $- \Sigma^-_\sigma$. If Λ^0 associated with the Σ^-_σ

is seen, it is also recorded.

3) $\bar{K}p \longrightarrow \pi^+\pi^-$ These are events in which the production $\Sigma^\pm$ is

too short to be seen since it decays almost immediately on production.

Because the π associated with production and the π

associated with decay each have momentum in the region of 180 MeV/C, it

is largely impossible to classify these events unambiguously into the

Σ^+ or the Σ^- channel.   Only at momenta above threshold for

the charge exchange process can these events arise from the close decay

of $\bar{K}^0$ - mesons.

4) $K^-P \longrightarrow \pi^-P$ These may be Σ^+ events where the Σ^+ decays

immediately by the proton mode or these are 0 - prong events with

the close decay of a Λ^0 hyperon. Unlike the " $\pi^+\pi^-$ " events,

the π^- from Λ^0 decay has momentum very different from that of

the π^- associated with Σ^+ production. Consequently, after

measurement by conventional means, or by use of template, at the scan

table, these events can be separated unambiguously into the Σ^+

and Λ^0 categories.

There are possible ambiguities in the classifications Σ_σ^- and $\pi^- \bar{p}$ if only scanning information is used. Events classified as Σ_σ^- will comprise those where the Σ^- is identified from the accompanying π^+ meson and where the Σ^- is seen not to decay. These events are largely those in which the Σ^- comes to rest and is absorbed producing a secondary event with neutral secondaries. However, because it is difficult to judge at the scantable, the Σ_σ^- category will include events where the produced Σ^- passes into a plastic window and is absorbed there. To resolve this ambiguity all Σ_σ^- events have been measured. However, as far as the determination of the ratio Γ is concerned it is not necessary to make a separation of the events.

For $\pi^- p$ events classified as Σ_p^+ decays with unseen Σ^+ there may be some contamination from events in which the Σ^+ passes into the perspex and is mistaken for a proton. Some of these may be resolved by the presence of an associated π^+ from Σ_π^+ decay. For Σ_p^+ the decay proton will come to rest in the plastic window and not be seen.

In determining the value of Γ at rest it is essential to divide the scanned events into those "at rest" and those "inflight". In general all events where the $\Sigma^\pm$ is visible can be unambiguously classified since events at rest all demonstrate accurate collinearity of the $\Sigma^\pm$ and the production $\pi^\pm$. Events in-flight show lack of collinearity except for those events in which the Σ and π are produced at small angles to the direction of flight of the kaon. Then the lorentz transformation leads to a geometry of that event which simulates collinearity. However, from the results of separation into events at rest and in-flight (which occur in a ratio, see later, of about 17.5%) the proportion of in-flight events which can simulate these at rest through collinearity is at most 0.5% of the genuine events at rest. Moreover, events of this kind (i.e. collinearity where Σ and π are produced at small angle to the K) were checked with a template which was

made up of an average profile of kaons coming to rest and producing collinearity at right angles to the kaon track. This proved to be an effective way of separating those events ambiguous between at rest and in-flight. Of course the "$\pi^+\pi^-$" and "π^-p" events can only be judged to be at rest (or in-flight) by use of the template.

b)   Recording of scan data through Scan Codes

Events selected as above were recorded as follows. A ten digit number is used with meanings defined as below.

X	Y	A	B	C	D	E	F	G	H

x,y   =   Zone in fiducial volume where the events is found.

The other digits A to F are zero except for:-

A   =   prong size of primary vertex

B   =   1 for Σ^-

         2 for Σ^+

C   =   1 for collinearity of Σ and π

     =   2 for non-collinearity

     =   3 for uncertain collinearity.

D   =   1 for proton decay of Σ^+

     =   2 for pion decay of $\Sigma^{\pm}$

     =   3 if no decay. This could describe a Σ^- which is absorbed or

          indeed $\Sigma^{\pm}$ passing into the perspex window before decaying.

E   =   1 for $\pi^+\pi^-$ event

     =   2 for $\pi^- p$ event

F   =   1 for associated Λ^o

     =   2 for associated K^o

G   =   not used

H   =   1 if the event is preceded by a 2-prong elastic K scatter.

For example codings for common events produced by kaons at rest   are:-

22110000 - $\Sigma_p^+ \pi^-$ (collinear)

22120000 - $\Sigma_\pi^+ \pi^-$ "

21120000 - $\Sigma_\pi^- \pi^+$

21130000 - $\Sigma_\sigma^- \pi^+$ (Σ^- without decay)

21130010 - $\Sigma_\sigma^- \pi^+$ (Σ^- absorbed in the reaction $\Sigma^- p \longrightarrow \Lambda^0 n$)

2000100 - $\pi^+ \pi^-$ event

2000200 - $\pi^- p$ event

The code is invaluable for selecting events from the master list of scanned events on magnetic tape.

3.2 Results of Scanning

Scanning Efficiencies

In order to evaluate the scanning efficiencies, films were scanned twice in this experiment independently.   Differences were resolved in a third scan.   The events were classified into the following categories:

1 - N_{12} Events found in both scans,

2 - N_1 Events found   in the first scan

3 - N_2 Events found   in the second scan

4 - N_T True (unknown) number of events on the films.

If λ_1 and λ_2 are the individual scanning efficencies as defined by the expressions

$$\lambda_1 = N_1/N_T \quad \text{and} \quad \lambda_2 = N_2/N_T \qquad \dots\dots\dots\dots\dots(29)$$

Then $\lambda_1 \cdot \lambda_2$ is the probability that an event will be seen in both scans.   Then:-

The number of events found in both scans is

$$N_{12} = \lambda_1 \cdot \lambda_2 \cdot N_T \qquad \dots\dots\dots\dots\dots(30)$$

solving equations (29), (30)

$$\lambda_1 = N_{12}/N_2 \ , \ \lambda_2 = N_{12}/N_1 \qquad \dots\dots\dots (31)$$

and

$$N_T = N_1 \cdot N_2 / N_{12} \qquad \dots\dots\dots (32)$$

The probability that scanners 1, and 2 will both miss an event should be given by:

$$q = (1 - \lambda_1)(1 - \lambda_2) \qquad \dots\dots\dots (33)$$

Then the combined efficiencies over two scans should be

$$\lambda_c = 1 - (1 - \lambda_1)(1 - \lambda_2) \qquad \dots\dots\dots (34)$$

$$= \lambda_1 + \lambda_2 - \lambda_1 \cdot \lambda_2$$

3.3   Measurement of events

The measurements were carried out on image plane digitized machines where the accuracy, corresponding to helix fit errors on the film was about 8μ for track measurements and about 10μ on fiducial cross measurements. Because small angle scattering of the primary kaon is quite probable, 15 points were measured on each primary to detect scattering. Such primaries are failed by the on-line measuring system and so the primary track has to be reduced in length to remove the scatter and measured until the primary is accepted.   In this way a scattering was not allowed to bias the measured curvature of the track.   A scattering very close to the primary interaction would lead to the event becoming unmeasurable.

The measurements were processed by the GEOMETRY and KINEMATICS programmes which had been modified:-

a)   to take account of the geometry of the T.S.T. system and the measurement of γ rays (reference 13).

b)   to allow for fitting of events in KINEMATICS where the primary is stopping (reference 14).   If the measured momentum of the K primary is in excess of 50 meV/c, then standard KINEMATICS

is used. Below this momentum, the fitting routine of KINEMATICS
is modified to take into account the increasing lack of dependence
of the momentum of the vertex on the measured momentum of the
midpoint of the track.

The pass rate in GEOMETRY is about 80% and in KINEMATICS a further
80%,leading to an overall pass rate of about 64%. After measurement,
events which have failed were re-examined (judged) on the scan table to
decide if the event should be remeasured. The main category of failures
comprised events with short straight tracks which result from the shallow
depth of the T.S.T. In all there were 3 passes of the unsuccessful events
through the measuring/processing chain. The total, overall pass rate
from measurement through to KINEMATICS is 98%. The scanning/measuring
sytem is summarised in figure 8. Two groups of measurements were made.

i)   The first of these consisted of all $\pi^+\pi^-$ and π^-p events. Here
     the aim of the measurement was to

     a)   check the division of these events into "at rest" and"in
          flight" categories previously judged by the template,

     b)   to resolve these π^-p events, which were not resolved by
          template, into Σ^+ and Λ categories.

ii) The second group comprised all events judged to be in-flight to
     provide data for the cross-sections of in-flight interactions and
     particularly for the variation of the quantity Γ with energy.

3.4.   Results of measurements

a)   General results on beam momenta

     Beam momenta can be determined at two stages. The first is at the
end of the GEOMETRY programme where the momentum corresponding to the helix
fitted to the measured points is available. The second is at the end of
KINEMATICS where if this momentum has been "pulled" to a new value with

FIG. 8 EVENT PROCESSING CHAIN

higher precision by the fitting procedures.

Since the "pulling" in the fitting procedures varies with the tightness of the constraints in the fitting, then for example, a comparison of $\pi^+\pi^-$(unconstrained fits) with Σ^+_π (highly constrained fits) should be made at the end of GEOMETRY and not after KINEMATICS. The reasons for this are quite clear in the figures below.

i)   Collinear events (Σ^-_π , Σ^+_π and Σ^+_p)

The distribution of beam momentum is expected to be close to zero momentum for these collinear (hence stopping kaon) events. As can be seen in figure 9 the beam momentum after GEOMETRY shows a spike at zero momentum which corresponds to all primary kaons whose measured momentum at the midpoint of the track is less than that expected from the range of the track ("overstopped" kaon). There is a second group distributed about 100 Mev/c. When these events pass through the fitting routines of KINEMATICS the momentum is pulled as expected towards zero.

This is clearly seen in figure 10. In general these fitted momenta are less than 50 Mev/c and certainly less than 100 Mev/c.

ii)   Non-collinear events (Σ^-_π , Σ^+_π , and Σ^+_p)

The non-collinearity of these events implies that they are not at rest. The beam momentum from GEOMETRY figure 11 is now distributed about 200 Mev/c, that from KINEMATICS, figure 12 no longer shows the pulling towards zero momentum.

iii) At rest and in flight events ($\pi^-\pi^+$ and π^-p)

The distribution of beam momentum from GEOMETRY, figures 13,14, is now little different from that from KINEMATICS although these events do fit the unphysical (strangeness not conserved) channels $\pi^+\pi^-n$ and $\pi^-p\pi^0$. This is because the degree of constraint is low. However it is clear from a comparison of figures 10, 12,13,14 that this group of data contains both 'at rest' and 'in flight' interactions.

$$\bar{K} P \longrightarrow \Sigma^{\pm} \bar{\pi}, \Sigma^{+} \longrightarrow P\pi^{0}$$
$$\bar{K} P \longrightarrow \Sigma^{+} \bar{\pi}, \Sigma^{+} \longrightarrow h\pi^{+}$$
$$\bar{K} P \longrightarrow \bar{\Sigma}^{-} \bar{\pi}, \bar{\Sigma}^{-} \longrightarrow n\pi^{-}$$

COLLINEAR EVENTS

FREQUENCY

FIG. 9 UNFITTED BEAM MOMENTUM DISTRIBUTION

BEAM MOMENTUM GEV/C

FREQUENCY

$\bar{K}P \longrightarrow \Sigma^{\pm} \pi^{\mp}, \Sigma^{+} \longrightarrow P\pi^{0}$
$\bar{K}P \longrightarrow \Sigma^{\pm} \pi^{\mp}, \Sigma^{\pm} \longrightarrow n\pi^{+}$
$\bar{K}P \longrightarrow \bar{\Sigma}\pi^{+}, \bar{\Sigma}^{-} \longrightarrow n\pi^{-}$
COLLINEAR EVENTS
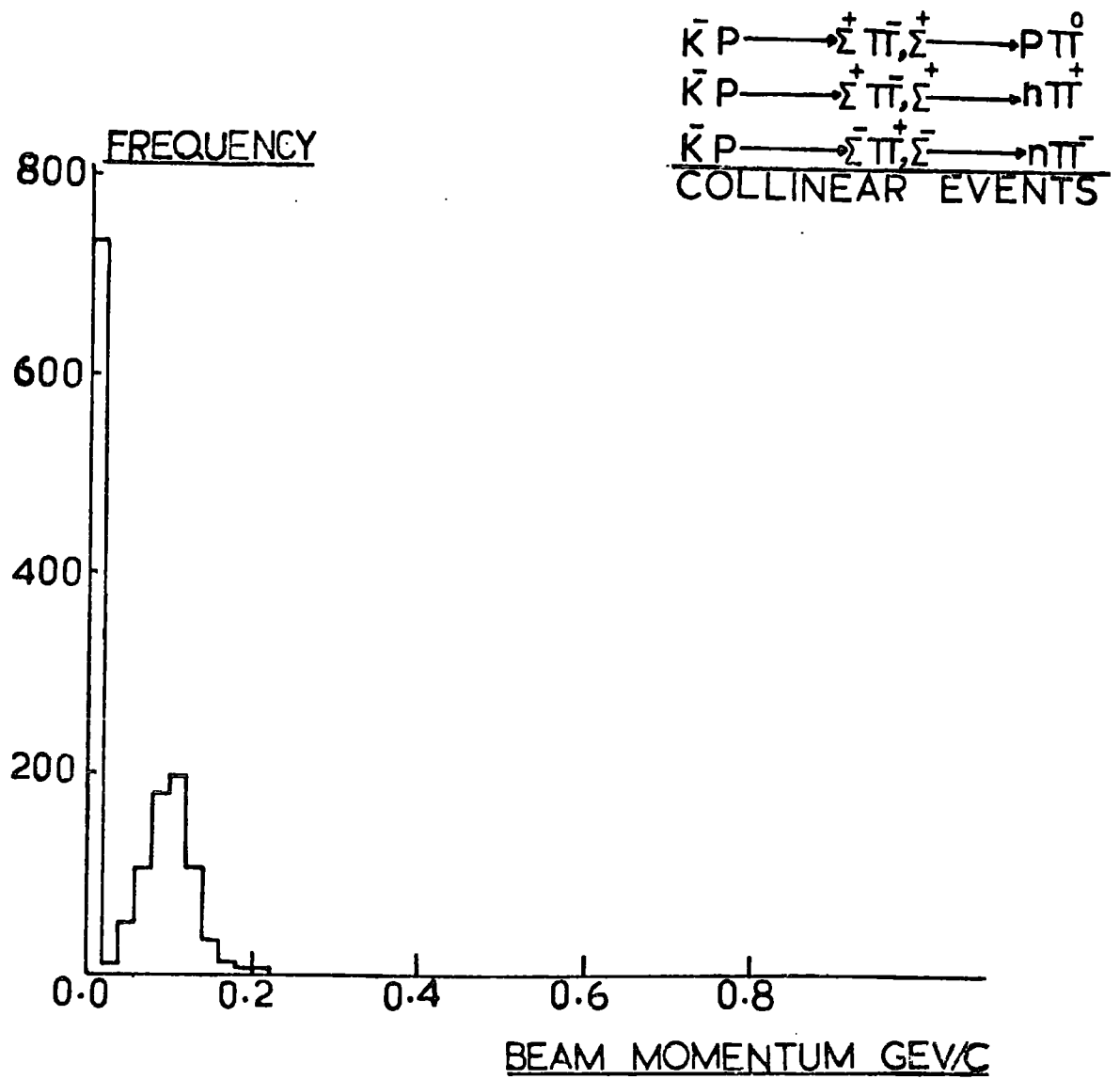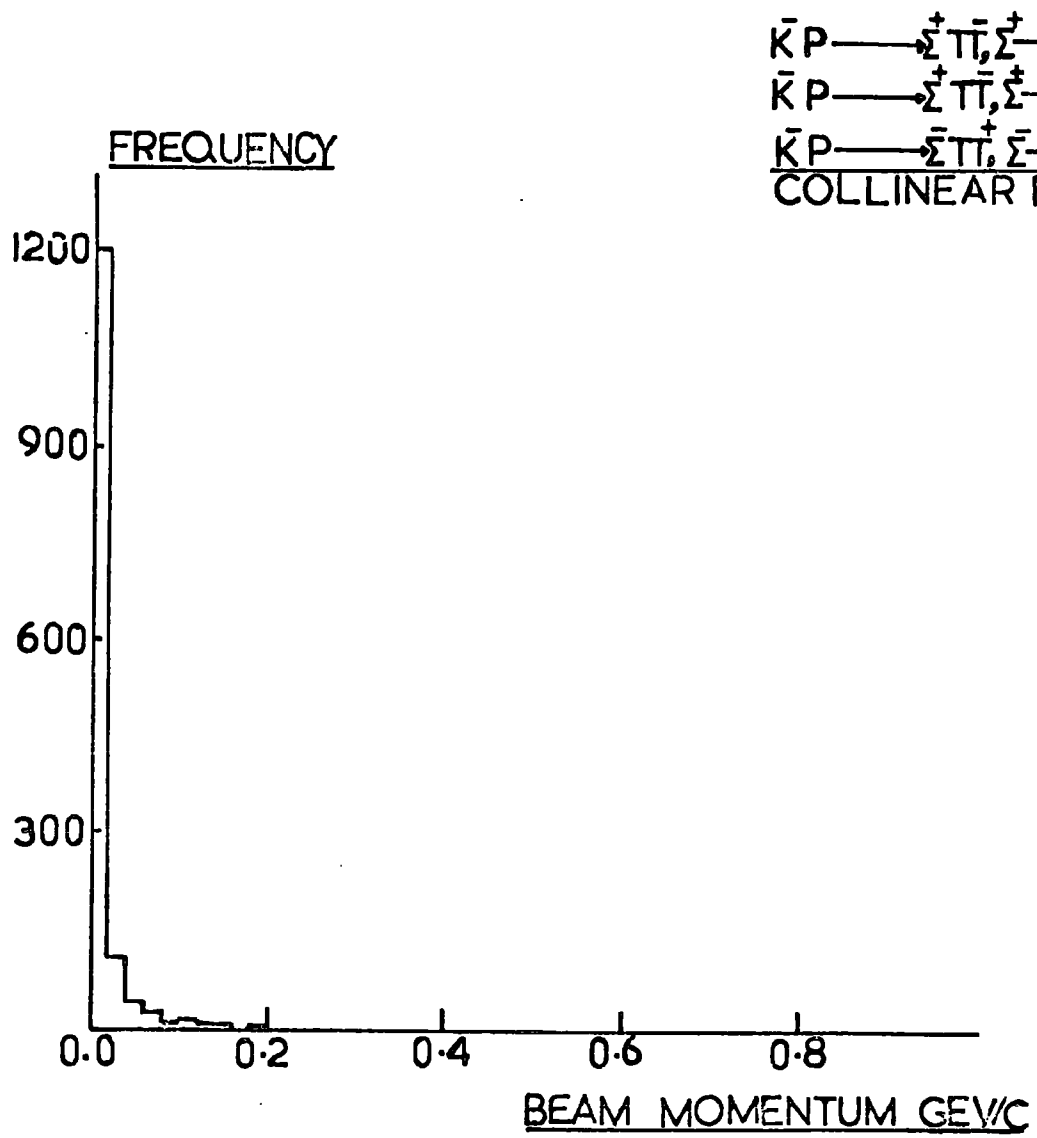
BEAM MOMENTUM GEV/C

FIG. 10 FITTED BEAM MOMENTUM DISTRIBUTION

$$\bar{K}P \longrightarrow \Sigma^+\pi^-, \Sigma^+ \longrightarrow P\pi^0$$
$$\bar{K}P \longrightarrow \Sigma^+\pi^-, \Sigma^+ \longrightarrow n\pi^+$$
$$\bar{K}P \longrightarrow \Sigma^-\pi^+, \Sigma^- \longrightarrow n\pi^-$$

NON COLLINEAR EVENTS
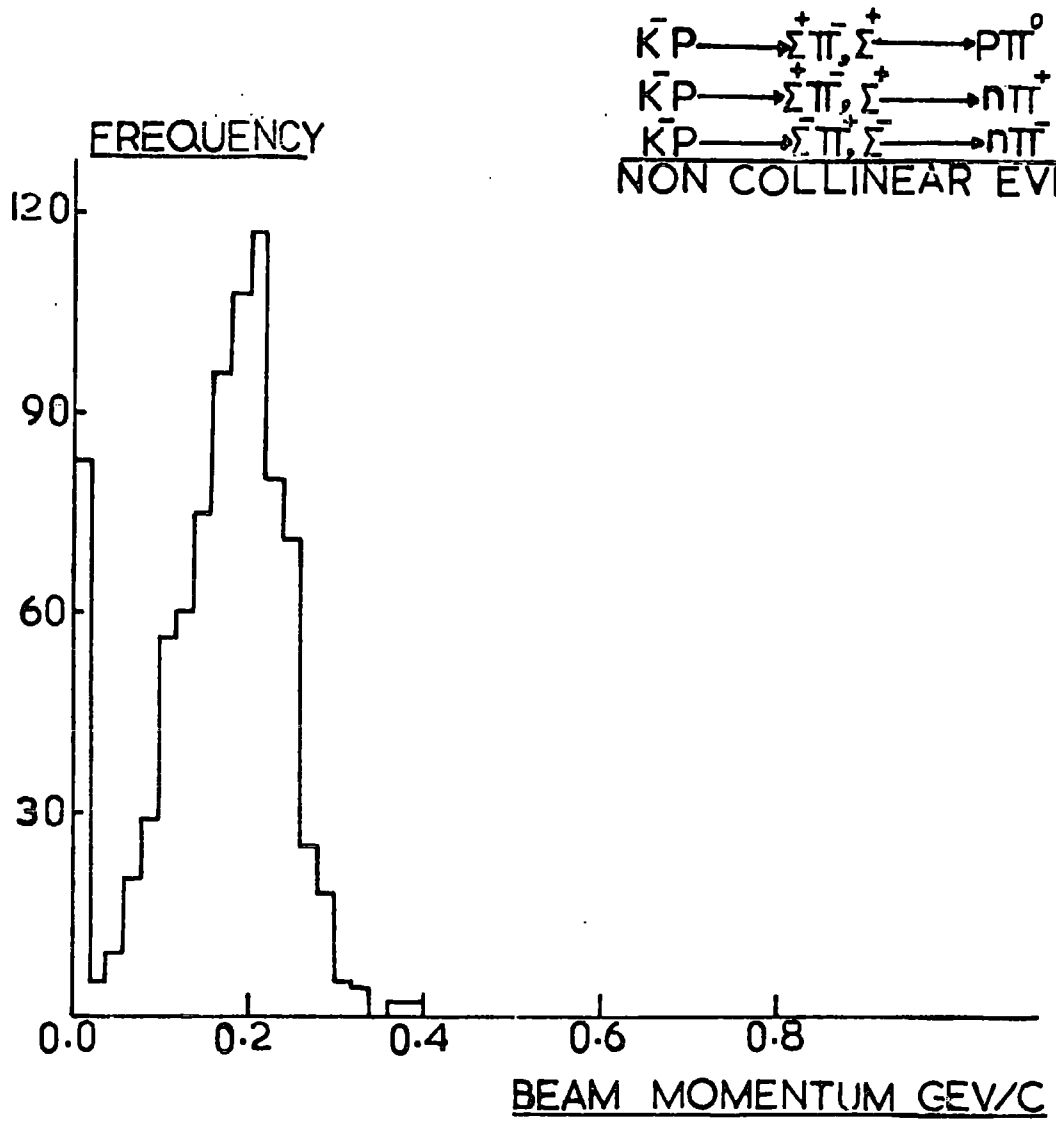
FIG.11 UNFITTED BEAM MOMENTUM DISTRIBUTION

$K P \longrightarrow \Sigma^+ \pi, \Sigma^+ \longrightarrow P \pi^0$

$K P \longrightarrow \Sigma^+ \pi, \Sigma^+ \longrightarrow n \pi^+$

$K P \longrightarrow \Sigma^- \pi, \Sigma^+ \longrightarrow n \pi^-$

NON COLLINEAR EVENTS
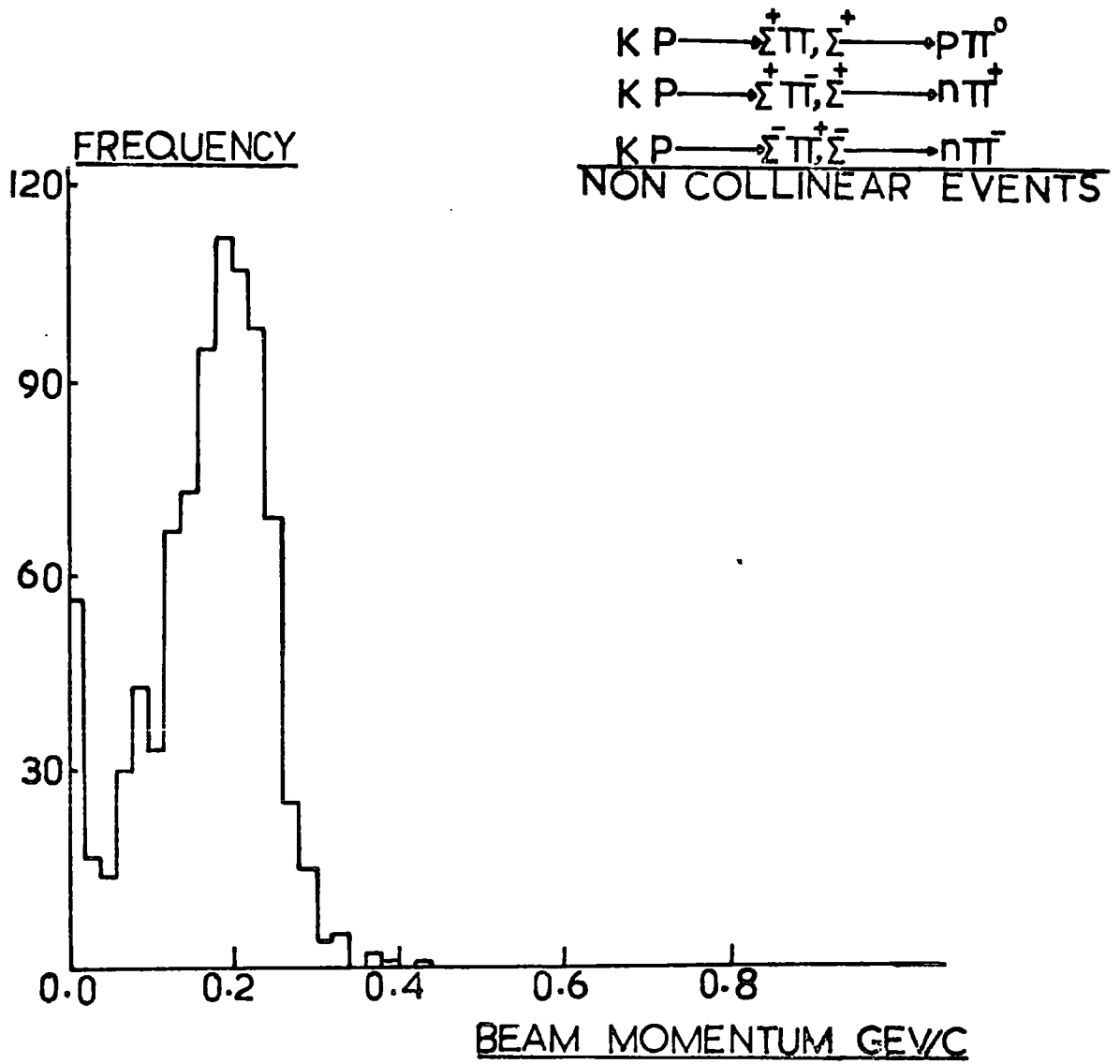
FIG 12 FITTED BEAM MOMENTUM DISTRIBUTION
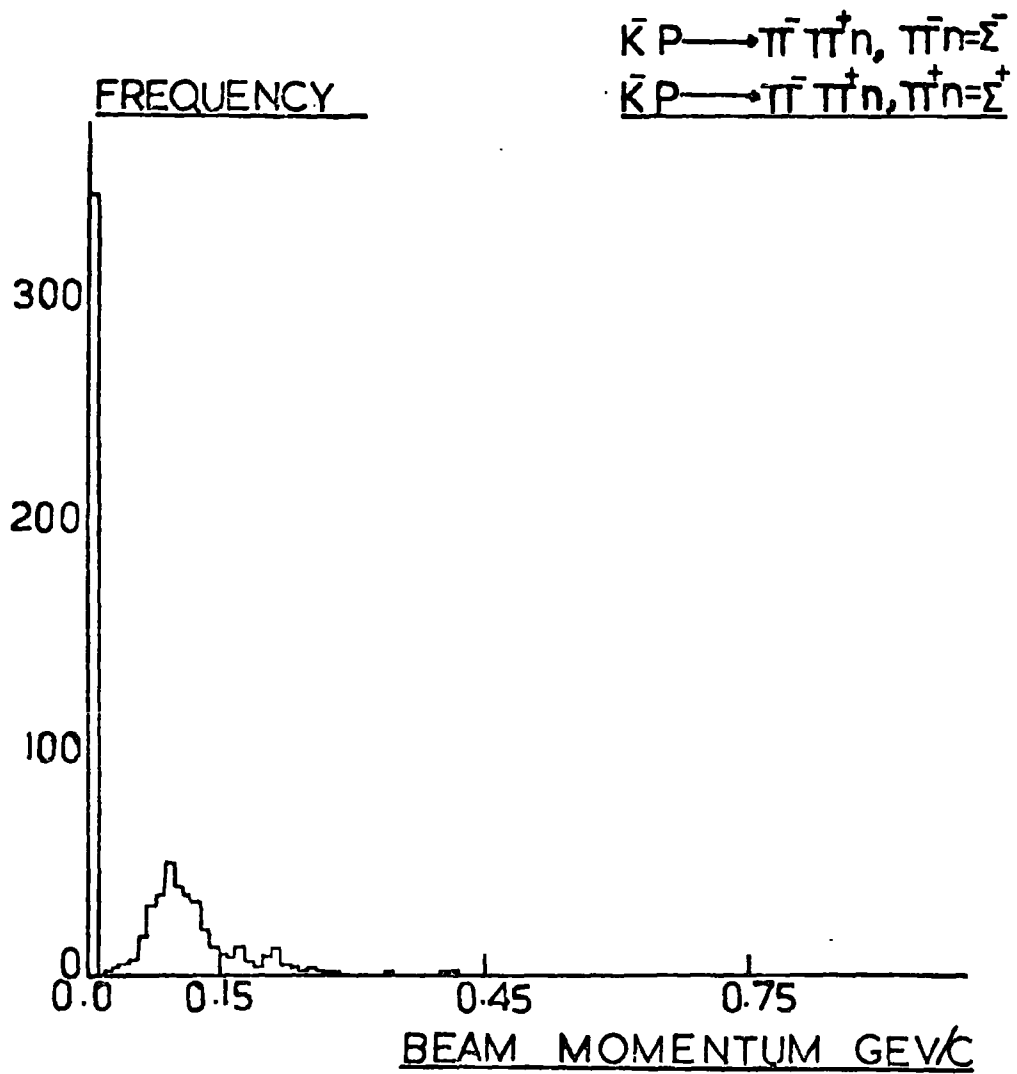
FIG. 13 UNFITTED BEAM MOMENTUM DISTRIBUTION

$K P \longrightarrow \pi^- P \pi^0, \pi^- P = \Lambda^0$

$\bar{K} P \longrightarrow \pi^- P \pi^0, \pi^- P = \Sigma^+$
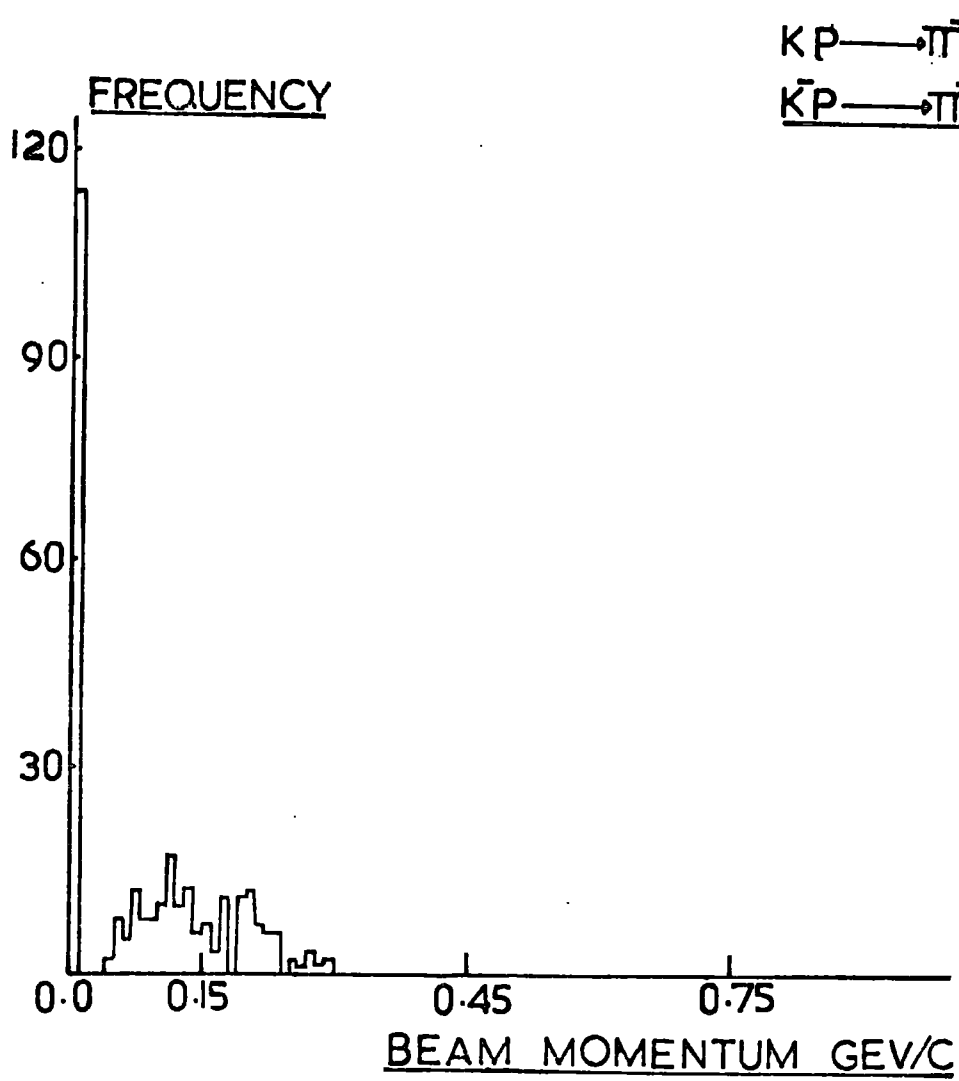
FIG.14 UNFITTED BEAM MOMENTUM DISTRIBUTION

b)   Resolution of $\pi^+\pi^-$ and π^-P events into the "at rest" category

To separate the "at rest" group a comparison is made of the distribution of beam momentum with that for collinear events.   Each shows a spike of zero.   It has to be assumed that this spike corresponds to primaries which are exactly at rest.   Normalising to the collinear events, then the number of "at rest" $\pi^+\pi^-$ (or π^-P) events whose measured momenta are in the region of $\sim$ 100 Mev/c can be calculated.   The difference between the calculated and observed values is the number of events in-flight.

It is clear from figure 11 for non-collinear (in-flight) events, that although the primaries interact in-flight, the distribution of measured momenta shows a spike at zero momentum.   Correspondingly the assumption made above in normalising the spikes of collinear and $\pi^+\pi^-$ or (π^-P) events is not completely valid.   This will have lead, above, to an over-estimation of the number of $\pi^+\pi^-$ (or π^-P) events at rest.

A separation has also been made by using a template to judge whether the primary is at rest.   The template was checked against collinear and non-collinear events which suggests that at most 2% of those primaries judged to be at rest are in fact in-flight.

Both methods of judging at rest events are compared in tables (3 and 4).   Because of the uncertainty of the first method, judgement of "at rest" by template is preferred and this method only is used subsequently.

c)   Resolution of π^-P into Λ^0 and Σ^+ categories

Whereas the use of a template appears to be the best method of resolving whether the primary of an interaction was at rest or in-flight, this does not appear to be so for judging whether a π^-P event is due to the production and decay of a very short-lived Λ^0 or Σ^+.

In principle the momentum of the negative pion produced in association

COMPARISON BETWEEN EVENTS AT REST AND IN FLIGHT USING

a) Template

TABLE. 3.

$\pi^+\pi^-$ (TOTAL SAMPLE) =822		$\pi^- P$ (TOTAL SAMPLE) =406	
AT REST	IN_FLIGHT	AT REST	IN_FLIGHT
84.9%	15.08%	71.8%	28.8%

b) Measurement

TABLE. 4.

$\pi^+\pi^-$ (TOTAL SAMPLE) =701		$\pi^- P$ (TOTAL SAMPLE) =289	
AT REST	IN_FLIGHT	AT REST	IN_FLIGHT
94.9%	5.04%	76.5%	23.47%

with the Σ^+ or in the decay of the Λ^0 is sufficient to resolve these categories. For example, the momentum of the produced pion is about 180 Mev/c for the Σ^+ and is below 140 Mev/c for the Λ^0 . Templates drawn to curvatures corresponding to these momenta should lead to adequate resolution where there is sufficient pion length, discrimination by the template is possible but this occurs in approximately 63% of the events.

For the remainder, although the track length is too short for resolution by template, measurement leads to the separation of events.

In a sample of about 55% of all $\pi^- p$ events (judged to be at rest) that were measured it is possible to estimate the proportions which are due to Σ^+ and to Λ . The events are plotted in figure 15 where for each event the pion momentum and the opening angle between the pion and the proton are shown. The data divide clearly into two groups, one centred on the expected momentum of 180 Mev/c for Σ^+ and the other clustered about the kinematically expected relation between the pion momentum and opening angle for the relation for the reaction $K^- P(\text{at rest}) \longrightarrow \Lambda \pi^0.$ The corresponding relation for the reaction $K^- P \longrightarrow \Sigma^0 \pi^0$ leads to lower pion momenta. From this plot the proportion of events due to Σ^+ decay is estimated to be $(73 \pm 7.9\%)$. This figure is then applied to the whole sample.

A small number of the so-called $\pi^- p$ events arise in fact from $\pi^- \Sigma^+$ events where the short Σ^+ passes into the target wall decays there. For pion mode of decay the probability that the pion emerges from the wall is estimated by Monte Carlo calculations, to be as high as 95%. Prior to the measurements above all of the so-called $\pi^- p$ events were scrutinized and 10 were found to have associated pions. These have been transferred to the Σ^+_π class.

d) $\underline{\Sigma^- \sigma}$ events

These events were measured for two purposes. One is to determine the range of the absorbed Σ^- since this will provide a check on the range momentum relation that is used in GEOMETRY and KINEMATICS. The second

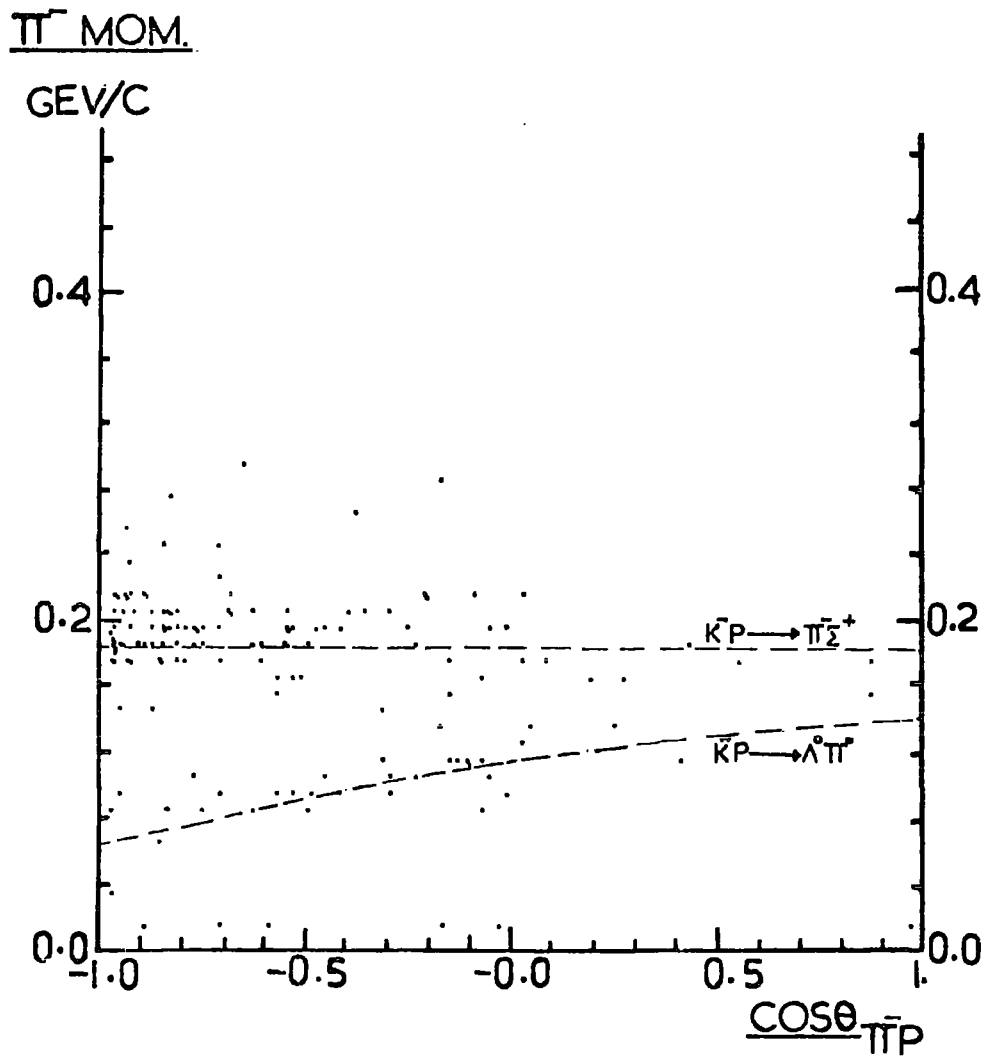## $\overline{\pi}P$ EVENTS AT REST (BY TEMPLATE)

FIG.15. MOMENTUM OF NEGATIVE PION AGAINST THE OPENING ANGLE BETWEEN THE PION AND THE PROTON

purpose is to determine, what proportion of the events were due to the Σ^- entering the plastic.

The average range if found to be $(1.19^{\pm} 0.05)$ cm and this confirms the correctness of the range momentum tables used. The number of events terminating in the perspex is found to be about 8%. As pointed out in section 3.1.a these terminating events do not affect the determination of Γ.

3.5 Final classification of events

To summarise, events have been classified into at rest and in-flight largely by the collinearity of the events and in a small number of cases by the use of a template. These events have been further divided into physical channels. In a relatively small number of cases measurements have been used to resolve ambiguities. The results of the scanning and the classification of the data produced in Durham are shown in detail in table 5. The scanning efficiencies from a double scan (plus a check scan) are all found to be high. These events together with the events from the collaborators at Brussels, UCL, and Warsaw are gathered together and discussed in chapter 4.

TABLE. 5.

CLASSES	AT REST&INFLIGHT		AT REST		INFLIGHT	
	TOTAL NUMBER OF EVENTS	EFFICIENCIES	TOTAL NUMBER OF EVENTS	EFFICIENCIES	TOTAL NUMBER OF EVENTS	EFFICIENCIES
Σ^-_π	4856	97.91	4271	99.95	585	99.96
Σ^-_σ	643	97.89	560	99.94	83	99.95
Σ^+_π	1290	97.91	1035	99.95	255	99.96
Σ^+_P	1229	97.81	1010	99.95	219	99.86
$\pi^+\pi^-$	822	97.51	698	99.84	124	99.67
$\pi^- P_{(\Lambda)}$	123.4	94.9	93.4	99.4	30	97.46
$\pi^- P_{(\Sigma)}$	291.6		204.6		87	
K^o	140					89.25

THE TOTAL EFFICIENCY FOR AT REST SAMPLE=99.93

THE TOTAL EFFICIENCY FOR INFLIGHT SAMPLE=99.967

CHAPTER FOUR   DETERMINATION OF THE $\bar{\Sigma}/\Sigma^+$ PRODUCTION RATIO AND THE Σ^+ DECAY BRANCHING RATIO

4.1   Total available data

Altogether in the collaboration between the groups of Brussels, Durham, University College London and Warsaw about 22354 events have been found by careful scanning and check scanning.   A breakdown of the total data is presented in table 6 in two forms.

Firstly the data is presented in the form for use in method 1, which is the method which relies largely on the accurate identification of the proton mode of decay of the Σ^+ but not on the separation of the pion modes of decay of the Σ^+ and Σ^- .   A subset of these data was scanned in which the separation of the pion modes was pushed to its limit. This means that events were further scrutinized and separated into Σ^+ and Σ^- categories.   These data were used in method 2.   All the data have been corrected for scanning efficiency and in flight events as in table 5.

4.2   Determination of Γ

The two methods referred to above have been described in detail in chapter 1.   In the first of these the branching ratio of the pion and proton modes of decay of the Σ^+ is assumed in determing Γ , in the second, both the branching ratio and the value of Γ are determined.

a)   Method 1

The advantages of this method are:-

(1)   It is independent of the separation of $\pi^+\pi^-$ events into those from Σ^+ and from Σ^- hyperons respectively.

(2)   It is independent of the mistaken classification of Σ^- events as Σ^-_π events.

(3)   That the precision depends upon the number of Σ^+_p events. These are readily identifiable at scanning time.

FINAL RESULT FROM THE COLLABORATION

TABLE 6.

DATA FOR METHOD 1

CLASSES	$\Sigma^-_\pi + \Sigma^+_\pi + \Sigma^+_\sigma + \pi^+\pi^-$	Σ^+_P	TOTAL
NUMBER OF EVENTS	18905	3449	22354

DATA FOR METHOD 2

CLASSES	Σ^-	Σ^-_σ	Σ^+_π	Σ^+_P	$\pi^+\pi^-$	TOTAL
NUMBER OF EVENTS	8505.5	1070.1	1862.8	2216.6	948.9	14603.9

Then the total number of Σ^- — hyperon produced by kaons is

$$N^- = N_{\Sigma_\sigma}(obs) + N_{\Sigma_\pi^-}(obs) + N_{\Sigma_\pi}^+(obs) + N_{\pi\pi}(obs) - \frac{B(N^+)}{1-B} \quad \ldots\ldots (22)$$

and the total number of Σ^+ — hyperon is

$$N^+ = \frac{N_{\Sigma_p}^+(obs) + N_{\pi p}^-}{1-B} \quad \ldots\ldots(16)$$

Using the number given in table 6a and the branching ratio, B, from the Paricle Data Group Tables (B=0.4835$^+$ 0.007) ,ratio Γ is just N^-/N^+ and is found to be

$$\Gamma = (\ 2.35^+\ 0.07\ )$$

b)   Method 2

Table 6b shows the numbers of events in the scanning channels used in this determination of Γ .   These numbers include the corrections which were discussed in sections 3.3. and 3.4.   No events have been rejected by selection criteria.   In this method, it is assumed that the ability to distinguish the sign of the charge of a Σ — hyperon should depend only upon whether the Σ track can be resolved, so that the recoil pion can be identified and its charge determined.   If the short distance ,r, is defined as the minimum effective length needed to detect the charge of the hyperon then the number of Σ— hyperons decaying by the pion modes in a distance r and which will appear as $\pi^+\pi^-$ events is shown by equation 27. (see chapter 1 and below).   From the numbers of $\pi^+\pi^-$ events in table 6b the cut off length r can thus be determined.   When it, and other data from table 6b, are substituted into equations 25 and 28 then the Γ ratio and the branching ratio B of the Σ^+ can be determined:

$$N(r) = (N_\sigma^- + N_\pi^-)(e^{t^-(r)/\tau^-} - 1) + N_\pi^+(e^{t^+(r)/\tau^+} - 1) \quad \ldots\ldots\ldots(27)$$

$$\Gamma(r) = \frac{(N_\sigma^- + N_\pi^-)(e^{t^-(r)/\tau^-})}{N_p^+ + N_\pi^+(e^{t^+(r)/\tau^+})} \quad \ldots\ldots\ldots(25)$$

$$B = \frac{N_{\pi}^+ \; e^{t^+(r)/\tau^+}}{N_p^+ + N_{\pi}^+ e^{t^+(r)/\tau^+}} \qquad \ldots\ldots\ldots\ldots(28)$$

The above equations allow, by interpolation, to find the effective range, r, which applies to the scanning of this experiment and the values of Γ and B.

These values are:

$$r \quad = \quad 0.045 \text{ cm}$$
$$\Gamma \quad = \quad 2.38^{+}_{-} \, 0.04$$
$$B \quad = \quad 0.487^{+}_{-}0.008$$

4.3. Critique of methods for Determining Γ

A summary of the previous determinations of Γ is given in table 7. Only those of Kim, Tovee and the present work are of sufficient precision to warrant further discussion. Superficially, previous methods which have used bubble chamber and nuclear emulsion techniques to determine Γ are similar. In both, events are selected for analysis which are judged to be the production of $\Sigma^{\pm}\pi^{\mp}$ in kaon interaction at rest on proton because the tracks of the produced $\Sigma\pi$ particles are collinear. However the composition of the events, as seen below, differ considerably and in these differences the disparity of the measured values of Γ must lie.

In the chamber the potential ranges of the produced $\Sigma^{\pm}$ hyperons are about 1.05 and 1.26 cm respectively. As these are long compared to the decay lengths then about 93% of the Σ hyperons decay in flight. If the decay occurs in the first 0.5 to 1mm of the path of the Σ, the hyperon is not seen. A correction for the loss of events over the short, but not very well known, distance has to be made. The effect of measuring error on this small distance leads to over correction where the lifetime is very short. Consequently the measured value of $\Gamma = \Sigma^-/\Sigma^+$ will be reduced.

In the emulsion there is no magnetic field to determine the sign of the charge of the Σ — hyperon. However with potential ranges of 0.06 to

TABLE(7)

DETERMINATION OF THE Σ^-/Σ^+ PRODUCTION RATIO BY K MESON CAPTURES AT REST

Author	Γ
Humphrey and Ross(ref:2)	2.15 ±0.12
Kim(ref:1)	2.06±0.06
Eisele(ref:8)	2.2 ±0.1
Value deduced from Chang's data(ref:7)	2.29±0.11
Tovee(ref:5)	2.34±0.08
This experiment	2.35±0.07

0.08cm most hyperons (about 82%) come to rest where the signatures for charge are clear (Σ^- hyperons are absorbed, Σ^+ hyperons decay collinearlly into protons of characteristic range or into pions of characteristic ionisation). Consequently only those Σ hyperons can be employed in the analysis which have stopped and a correction for the approximately 18%, events in flight has to be made. In this case the distances over which the corrections are to be made are quite precise, and relating these distances to proper times is also precise.

On balance the emulsion method is freer of systematic effects than previous bubble experiments and hence the result of Tovee is to be preferred to that of Kim. This conclusion is fully supported by the work described in this thesis which is independent of lifetime correction. It relies heavily on the classification of events at scanning time and hence calls for high scanning efficiency and judgement.

A further indication that the Kim value is in error is provided by an analysis of A.D.Martin (reference 15) who has carried out a determination of the coupling constant $g_{KN\Lambda}$ and $g_{KN\Sigma}$ by means of relating KN amplitudes by dispersion relations. An important conclusion is that the low momentum data (provided almost entirely by Kim) is probably in error by as much as 20%.

The advantage of the present methods is that selection criteria (such as those quoted by Eisele have been avoided and consequently their associated systematic effects do not feature in the final results. However, it should be pointed out that in method 2 the effective length , r, that is determined is effective. in two senses. Firstly there is no absolute cut off length but a spectrum of lengths which vary with the geometry of the events and with observers . Secondly, this effective length is non physical in that, it is cut off length corresponding to zero measuring errors (see table 1). In other words above this length all events are resolved, below they are not.

In method 1 the difficulties above are avoided but the method
relies heavily on identifying Σ_p^+ decays. The majority of these
where the Σ itself is visible, present no problem at all and are already
separated from Σ_π^+ decays by the ionisation of the decay particle. However,
it was discussed in chapter 3, these events are contaminated by events where
$\Lambda-$ hyperons decay close to the production vertex.

Although the resolution of these events is good, any Λ decay left
in the sample will lead to a reduction of Γ .

4.4 Summary

It has been seen above that the determination of Γ and B are
consistent with one another. Compared to the two previous determinations
of Γ (with good statistics), it is clear that the present result is in
good agreement with the value of Tovee but not that of Kim. By taking a
weighted average of the Tovee value and the value in this thesis the follow-
ing value of Γ is obtained:

$$\Gamma = (\quad 2.35\pm0.05 \quad)$$

The value of the branching ratio,B, for the Σ^+ hyperon determining above
(0.487 ± 0.008) represents a new determination of this quantity with a precision
close to the existing world value. The closeness of our values of B to the
world value gives confidence in the determination of Γ value.

APPENDIX ONE

GEOMETRY Programme

The T.S.T. contains hydrogen whilst the main chamber volume is fitted with a mixture of neon and hydrogen. A geometrical programme HGEOM had been modified by (J.Guy) to reconstruct the tracks in the chamber and to allow for the extra media, consequently Range-momentum tables had been generated for the three media (hydrogen,perspex and neon-hydrogen). Other constants such as that for the coulomb scattering in the perspex must be provided and storage allocated in the geometry programme.

The track which leaves the hydrogen and goes into the neon is indicated by measuring the last point in hydrogen twice. However helix fittings were applied to the track sections so as to reconstruct them separately. Meanwhile a check was made to see if the track has crossed the perspex plane and returned into hydrogen. If so the second part of the track is ignored.

HGEOM provides centre of track variables ($\frac{1}{p}, \phi, \tan\lambda$) and their correllated errors which are the normal measured quantities used by the KINEMATIC fitting programme HKIN, further for the neon section of the track these 3 variables are swum to the mid point of hydrogen and a mean of these variables and those for hydrogen is taken. When the geometrical reconstructionof the bubble chamber event has taken place, the event must be tested against hypotheses of the nature of the event suggested by the experimenter. (KINEMATICS).

APPENDIX TWO

KINEMATICS Programme

By using the conservation laws of energy, momentum, charge....etc. the KINEMATIC programme attempts to identify uniquely the tracks for the reconstructed events.

Modification had been made to the KINEMATICS Programme to handle stopped K events. Fitting stopped K with ordinary KINEMATICS (i.e. the version used for in-flight fitting events) leads to a low pass rate e.g. on a sample of sigma-pion events, a pass rate of about 65% through KINEMATICS was obtained.

It is necessary to have a reliable fitting system in order to separate events at rest from those at low momentum (e.g. 100Mev/c) which have been essentially separated by template . A version of KINEMATICS fitting to Px, Py, Pz at the vertex instead of the variables ϕ , $\tan\lambda$, $1/p$ was introduced into subroutine ITERAT and this lead to a high pass rate, but also so difficult interpretation of the quality of the fits since the input errors are not Gaussian. However, the fitted values of K-momentum at the vertex did not show an improvement over the measured values. Moreover altering the constraint tolerances in the fitting did not lead to any effective improvement.

A further modification was made in fitting at rest events, such that standard KINEMATICS could be used. The variation of centre of track momentum depends on the change in vertex momentum through the range momentum relation and so the fitting routine of KINEMATICS was modified to take into account the increasing lack of such dependence at low momentum with an arbitrary function. The Swim routine was modified so that when the vertex momentum of the K is less than 50 Mev/c, the normally returned vertex slope is multiplied by the arbitrary function which is unity at p = 50 Mev/c and zero for P= 0 Mev/c. Results of modification to pass

rate was similar to those obtained from Px, Py, Pz but the stretch functions are now Gaussian and the fitted K-momentum distribution gives a much sharper peak at zero.

ACKNOWLEDGEMENTS

I would like to thank Professor A.W.Wolfendale who made available
the facilities of the Physics Department at Durham during my work for
this thesis.   My particular thanks go to my supervisor, Dr.J.V.Major
for the enormous amount of help and useful advice he has given and the
many interesting discussions we have had.

I would like to thank all the other members of the Higher Energy
Nuclear Physics Group at Durham for their many discussions during the
course of the work, particularly Mr.N.H.Bedford.   I am grateful to the
staff of the collaborating laboratories, particularly, Professor J.A.Zakrzewski
and Mr.J.Ciborowski.

My thanks are due to all the Scanning and Measuring Staff at
Durham University for their work on this experiment.

Lastly, but by no means least, I would like to thank my parents,
without their grants during my stay in England to study, this thesis would
not have been possible.

REFERENCES

Chapter One

1   J.K.Kim thesis, Columbia University (1966), (unpublished)

2   W.E.Humphrey and R.R.Ross, Phys.Rev.127, 1305 (1962)

3   R.H.Dalitz and S.F.Tuan, Ann.Phys.(New York) 10, 307, (1960)

4   A.D.Martin. Springer tracks in Mod.Phys.55 (1970), 142

5   D.Tovee, D.Davis, J.Simonovic, G.Bohm, J.Klabuhn,
        F.Wysotzki, M.C.Seithey-Barth, J.Wickens, T.Cantwell,
        C.Nighogain, A.Montwill, K.Garbowska-Priewska,
        T.Priewski and J.Zakrewski, Nucl.Phys.B33 (1971) 493.

6   M.Sakitt, T.B.Day, R.G.Glasser, N.Seeman, J.Friedman,
        W.E.Humphrey and R.R.Ross, Phys.Rev.139, 719, (1965)

7   C.Y.Chang, Phys.Rev.151 ,1081 (1966)

8   F.Eisele, H.Fitthuth,V.Hepp,W.Presser and G.Zech,2.Physick
        238,37e, (1970)

9   Particle Data Group (A.Rittenberg, A.Barbar-Galtieri,
        T.Lasinski, A.H.Rosenfeld, T.G.Trippe, M.Roes, C.Bricman,
        P.Soding, N.Barash-Schmidt and G.G.Wohl),Rev.Mod.Phys.
        43 part II, Si, (1971)

Chapter Two

10   C.M.Fisher. External Report. RL - 73-053

11   K.A.Kamakhy. Durham University Thesis (1973)

12   T.G.Coleman.Nucl.Inst.and Meth.107 (1973) 399

Chapter Three

13   J.Guy. Private Communication. R.L.

14   G.Fleming. Private Communication. Durham

Chapter Four

15   A.D.Martin, Phys.Lett.65B, 346 (1976)